Journal: GMD
Title: Global Simulation of Semivolatile Organic Compounds – Development and Evaluation of the MESSy Submodel SVOC(v1.0)
Author(s): Mega Octaviani et al.
MS No.: gmd-2019-19
MS Type: Model Description
Iteration: Revision

Reply to RC1

RC: This paper addresses the modeling of atmospheric PAH transport and chemistry/physics, which is certainly within the scope of GMD. It addresses some important processes for PAHs which have been, to the best of my knowledge, previously unresolved in models of its kind. This model built into the MESSy framework is a substantial contribution to the modeling of PAHs in the atmosphere. The methods are clearly outlined, and important assumptions are explicitly tested and discussed, leading to a reproducible work. The authors have given due emphasis to the existing literature, and their own contribution is clearly documented. The overall presentation of the paper is good, including language, adherence to title and abstract requirements, and formulae.

AR: We would like to thank the referee for his/her comments.

RC: The supporting information is very strong, but the code corresponding to the work appears to be not immediately accessible.

AR: SVOC will be available in the next official MESSy code release (version 2.55). Unfortunately due to the MESSy license conditions, we are unable to release the SVOC source codes as a publicly available electronic supplement. To access the codes, users are required to comply with the MESSy license and user agreement. More information is available on the MESSy Consortium website (https://www.messy-interface.org).

RC: L194: Soil density is a parameter of the capacity for PAH uptake. Is this density spatially specified? What is the origin of the value used (spatial database, land model or otherwise)?

AR: This study applied the global soil density data from Dunne and Willmott (1996) and the soil organic matter content from Batjes (1996). Both are available at a 0.5-degree grid resolution. These soil parameters vary spatially but not temporally. Soil density was based on sorptivity (Dunne and Willmott, 1996) whereas the organic matter content was based on regional measurements and empirical methods (Batjes, 1996). The two references have been added in the revised manuscript (see Line 387).

Dunne K.A., Willmott C.J. (1996) Global distribution of plant-extractable water capacity of soil, Int. J. Climatology 16, 841-859.

Batjes N.H. (1996) Total carbon and nitrogen in the soils of the world, Europ. J. Soil Sci. 47, 151-163.

RC: L201: Similarly to above, is the fraction of organic carbon in soil spatially varying? What is its origin?

AR: See above

RC: L215-220: Some clarifying statements on the application of volatilization from vegetation are warranted. Particularly, it is not clear to me how this CV is applied. Is the CV at 7 days after application used to calculate a timescale for complete revolatilization? i.e. to fit an exponential return to the atmosphere for deposited PAHs. Or is the fraction not volatilized after 7 days assumed to be permanently deposited? Also, is a single CV applied to all plant types?

AR: The volatilization rate from vegetation surfaces decreases with time. The rate obeys an exponential-time law and is determined by vapor pressure. The volatilization parameterization is based on fitting an empirical equation to observations of cumulated volatilizational losses of numerous pesticides over a period of 7 days after applications (Smit et al., 1998). In the model, this parameterization is applied for all plant types. The non-volatilized fraction is deposited (and subsequently accumulated and/or degraded).

Smit A.A.M.F.R., Leistra M., van den Berg F. (1998) Estimation method for the volatilization of pesticides from plants, Environmental Planning Bureau series 4, DLO Winand Staring Centre, Wageningen, the Netherlands, 101 pp.

RC: L255: The ocean is treated with comparatively little detail. Some discussion of how this could impact the strong bias of the model compared to measurements over the oceans would be informative. (Currently it is simply listed as a possible contributor to the bias)

AR: We thank the referee for the suggestion. We tried to add such information to improve the discussions. Additional texts are in:

- Subsection 2.2.5 Lines 260-267: "Sorption of SOCs in water to suspended particulate matter (colloidal or sinking detritus) is neglected. Therefore, SOC concentration in surface seawater and, hence, volatilization from sea surface is overestimated, in particular for very lipophilic (logKow > 6) substances. This bias is negligible for the substances studied here (PAHs) which are less lipophilic or volatilization is limited by vapor pressure (e.g., benzo(a)pyrene). Forces from strong winds, dissolved or particulate organics in seawater are transferred to air via sea spray, which adds to 265 particulate OM in air over the ocean (O'Dowd et al., 2008; Qureshi et al., 2009). This process is neglected in the model."
- Subsection 3.2.3 Lines 705-707: "BaP, mostly stays in the particulate phase, presumably also in seawater, therefore, may be somewhat underestimated due to the neglect of sea-spray driven aerosol suspension."

Nevertheless, we admit that the impact of neglecting ocean dynamics on model bias is complex and requires a further investigation.

O'Dowd C. D., Langmann B., Varghese S., Scannell C., Ceburnis D., Facchini M. C. (2008) A combined organic-inorganic sea-spray source function, Geophysical Research Letters, 35, L01 801, doi:10.1029/2007GL030331.

Qureshi A., MacLeod M., Hungerbühler K. (2009) Modeling aerosol suspension from soils and oceans as sources of micropollutants to air, Chemosphere, 77, 495–500, doi:10.1016/j.chemosphere.2009.07.051.

RC: L289-291: With a second-order representation, a higher value of kOH only suggests OH as the dominant loss pathway if concentrations of all three oxidants are equal. The concentration of OH would be expected to be much lower than the concentration of ozone, however.

AR: Experimental studies of reaction rates using typical concentrations of atmospheric oxidants indicate that the gas phase reaction with OH remains the dominant loss process for most PAHs (Keyte et al., 2013 and references therein). The average global OH concentration has been estimated to be 1.16×10^{6} molecules cm^{-3} (Spivakovsky et al., 2000). A reasonable ozone concentration range during day-time in the lower troposphere is 20–50 ppbv (at 298 K and 1 atm, 5×10^{11}–1×10^{12} molecules cm^{-3}). The experimental studies have reported small loss of 2-4 ring PAHs during exposure with high ozone concentrations ($\approx4\times10^{13}$ molecules cm^{-3}). k_{O3} was reported to be approximately eight orders of magnitude lower than k_{OH}.

Keyte I.J, Harrison R.M., Lammel G. (2013) Chemical reactivity and long-range transport potential of polycyclic aromatic hydrocarbons–A review, Chem. Soc. Rev. 42, 9333–9391.

Spivakovsky C.M., Logan J.A., Montzka S.A., Balkanski Y.J., Foreman-Fowler M., Jones D.B.A, et al. (2000) Three-dimensional climatological distribution of tropospheric OH: Update and evaluation. J. Geophys. Res. 105, 8931-8980.

RC: L314-316: The assumption of the rate doubling every 10 degrees is presented without reference. An explanation of the rationale behind this number should be included here.

AR: Following the referee's suggestion, the following sentence was added (see Lines 328-331): "The 10 K temperature warming is assumed to double the rate of degradation, following recommendations in chemicals risk assessment (European Commission, 2000) and consistent with findings, such as a two-time increase in the growth of hydrocarbon-degrading microbes in soils (Thibault and Elliott, 1979)."

European Commission: Guidance document on persistence in soil (2000), Technical Report 9188/VI/97 in relation to Council Directive No. 97/57/EC, EC Directorate General for Agriculture.

Thibault G.T., Elliott N.W. (1979) Accelerating the biological cleanup of hazardous materials spills. In Proc. Oil and Haz. Mater. Spills: Prevention-Control-Cleanup-Recovery-Disposal.

RC: L332: Why are gaseous reactions switched off for BaP?

AR: There is little significance of gaseous oxidation of BaP, as this substance mostly stays in the particulate phase. In addition, the reaction rate of BaP homogeneous oxidation remains poorly studied. This is mainly due to the experimental difficulty of studying the substance in the gas phase. Henceforth, the gaseous oxidation was switched off.

RC: L434-436: This output was selected as the single output for analysis, but other quantities could be analyzed using the same model experiments. Were any others investigated, and if so do they show similar behavior? I.e. are the factors affecting total PAH concentration representative of the factors affecting other outputs?

AR: The present study tries to quantify the response of model predictions to variation in emission interval, particulate-phase representation, the choice of gas-particle partitioning scheme, and volatilization. It is obvious that the changes in one or a few of these factors will cause a change in all model outputs. However, since emissions and volatilization are applied only at the surface, their direct effects may have little relevance to some of the outputs (e.g., atmospheric burden). We decided to perform the sensitivity analysis for near-surface concentrations, to allow us to evaluate the range of model bias in comparison to observations. However, in Section 3.1, we also presented shortly the direct effects of some of the factors to total deposition, partitioning coefficient, and lifetime, in order to support our discussion (see Lines 512-513 and Lines 555-559).

RC: L626-630: The CoV is compared between observations and model output. But the observations may not be representative of the same time-variations as the model. From the screening flowchart (Figure S3), it seems likely that many stations' "monthly" observations represent less than a full month's integration. This should make their monthly values more sensitive to synoptic-scale variations than their model counterparts, and much more sensitive to local-scale phenomena (e.g. convective precipitation and subsequent wet removal).

AR: We thank the referee for sharing his/her view. It is true that the monthly observation data at a few stations might be representative only for several days. Hence, they could be strongly linked to specific synoptic- and local-scale phenomena. Such influences would be less apparent in the model since the monthly mean values are used. However, the observations in Table 2 are represented as regional values, derived from pooling data from all stations in each region. This makes the impacts of synoptic- and local-scale variations associated with a specific station to the pooled data become less dominant, as the spatial extent increases and the time range varies across stations. Note that the ECMWF reanalysis dataset was applied to nudge the model meteorology, allowing the model to reflect the observed large-scale dynamics. Due to the reasons above, we may conclude that the CoV comparison is compatible and the differences between the model and observations are likely more model intrinsic than being induced by the time integration.

RC: L775-776: Does the underestimate follow the same pattern as SOA concentration? The omission of SOA in the model should be mentioned in the methods section.

AR: We thank the referee for the suggestion. The following sentence has been added: "It is noteworthy that the formation of secondary organic aerosols (SOA) from atmospheric oxidation and condensation of volatile organic compounds (VOCs) were not treated in the simulations. In the model, particulate organic matter is emitted and transported as a bulk aerosol species (OM)." (see Lines 371-374). PAHs may become trapped in OM, preventing them from evaporating to the gas phase and shielding them from chemical degradation. The omission of SOA as a source of OM is one contributing factor to the negative bias in predicted concentrations and particulate mass fraction. However, the underestimation may not follow the same distribution as SOA concentration. The multiphase reactivity of PAHs depends strongly on the phase state of organic coatings which is controlled by environmental

parameters such as temperature and relative humidity. Global simulations from Shiraiwa et al. (2017) indicate that SOA are mostly liquid in tropical, semi-solid in the mid-latitudes, and glassy solid in the middle and upper troposphere. The effectiveness of shielding by SOA is thus higher at cold and temperate regions, as well as in free and upper troposphere. These regions are not necessarily correlated with SOA-rich environments. The influence of this phase state on global predictions of BaP was discussed in a follow-up study by Mu et al. (2018).

Shiraiwa M., Li Y., Tsimpidi A.P., et al. (2017) Global distribution of particle phase state in atmospheric secondary organic aerosols. Nat. Commun. 8, 15002.

Mu Q., Shiraiwa M., Octaviani M., Ma N., Ding A., Su H., Lammel G., Pöschl U., and Cheng Y. (2018) Temperature effect on phase state and reactivity controls atmospheric multiphase chemistry and transport of PAHs, Sci. Adv. 4, doi:10.1126/sciadv.aap7314.

RC: L417: I believe this should read: "Two options for this factor were tested:"

AR: The sentence has been corrected (see Line 433).

RC: L435: The word "selected" is repeated.

AR: We removed "as the selected output" in the revised manuscript (see Line 451).

RC: L453-454: I believe that point (2) should be reworded. "...physically interpret." would be better than "...physically justify." if I understand correctly.

AR: We followed the referee's suggestion (see Line 469).

RC: L462: "are higher" should read "being higher" at the start of this line.

AR: The sentence has been corrected (see Line 477).

RC: L597: "On the contrary," should read "In contrast,"

AR: The sentence has been corrected (see Line 613).

RC: L618: "occur in the gas..." should be "occurring in the gas..."

AR: The sentence has been corrected (see Line 633).

RC: L645: "in a qualitative agreement" -> "in qualitative agreement"

AR: The sentence has been corrected (see Line 660).

RC: L714: "ocean shipping and do" -> "ocean shipping and does"

AR: The sentence has been corrected (see Line 698).

RC: L715: "potential origins" -> "potential point of origin"

AR: The sentence has been corrected (see Line 699).

Reply to RC2

RC: The paper describes modeling of the physical and chemical processes of PAHs in a global chemical transport model. Correctly modeling PAHs is important in addressing their adverse health impacts on both human being and the ecosystems. The topic is certainly within the scope of GMD and is of interest to the modeling community. The paper is well-written. I would recommend minor revision before accepted for publication.

AR: We thank the referee for his/her time and comments. Here we addressed all the comments.

RC: First of all, the title of the paper is "Global simulation of semi volatile organic compounds...". However, it appears that it was particularly developed for modeling PAHs so a more specific title should be used to reflect this. If the model is intended to be applied for other SVOCs, this should be clearly stated in the manuscript. Parameters for all other SVOCs treated by the model should be described and model evaluations should be performed.

AR: SVOC submodel was used here to simulate PAH compounds, as their physicochemical properties are well described and global emission inventory is available. The submodel was developed and is intended to be applied for the study of all potentially re-volatilizing and gas-particle partitioning (hence, semivolatile) compounds (e.g., PCDDs/Fs, PBDEs, novel brominated and phosphoric acid ester flame retardants, Diels-Alder organochlorine compounds) once their properties and emissions become apparent. In the revised manuscript, we included this statement in the introduction (see Lines 66-67). Further modifications might be deemed necessary, such as integrating new and improved parameterizations into SVOC.

RC: Regarding the "global" in the title of the paper, the main text does not even include a figure to show modeled global distributions. Land surface concentrations of PAHs in different regions (Asia, North American, etc.) have been published before so a global distribution plot would allow the reviewer to compare these with previous studies.

AR: The global distributions of PAH concentrations from the *base* experiment (f_0: annual emission + the *bulk* scheme + the Lohmann-Lammel scheme + no re-volatilization) are presented Fig. S4. In the revised manuscript, those from the *target* experiment (f_{1234}: i.e., seasonal emissions + the *modal* scheme + ppLFER scheme + with re-volatilization) were added (see Fig. S5).

RC: The authors did an excellent job of investigating the factors that affect the modeled concentrations. However, in my opinion, this is somewhat overkill because many parameters in the model detailed treatments carry large uncertainties. For example, the ppLFER scheme requires partitioning coefficients for more aerosol components. Uncertainties in these parameters may lead to a different judge on their impact on the predicted concentrations comparing to the base model.

AR: This study investigated the response of simulated concentrations to changes in the selected model factors. Studying uncertainty in the simulated concentrations resulting from the uncertainty in model input parameters could be an important factor, but is not an easy task and beyond the scope of this study. One previous work, i.e. Thackray et al. (2016) could be suitably followed for that purpose. The ppLFER model does not need more input data than available in the GMXe, hence, the off-line evaluation (Shahpoury et al 2016) of the parameterization suffices. As described in Section 2.2.2, each partition coefficient requires information on system parameters (Table S2) which are aerosol-system specific and solute descriptors (Table S6) which are substance specific. The partitioning coefficient is then parameterized as a function of temperature (for all aerosol systems) and humidity (for salts only). We argue any related uncertainty associated with the partitioning could lead to a different judge on the ppLFER impact on the predicted concentrations than what has been described in our study.

The accuracy of temporal variation of emissions can also be a source of uncertainty but we assume that they would have a limited effect on our coarse resolution and time averages. For future study, we would suggest more to test the sensitivity to neglect the SOA Formation.

Thackray C. P., Friedman C. L, Zhang Y, Selin N. E. (2015) Quantitative assessment of parametric uncertainty in Northern Hemisphere PAH concentrations. Environ. Sci. Technol. 49 (15), 9185-9193.

Shahpoury P., Lammel G., Albinet A., Sofuoğlu A., Domanoğlu Y., Sofuoğlu C.S., Wagner Z., Ždimal V. (2016) Evaluation of a conceptual model for gas-particle partitioning of polycyclic aromatic hydrocarbons using poly-parameter linear free energy relationships. Environ. Sci. Technol. 50, 12312-12319.

RC: The authors appear to imply that the model runs with the most sophisticated treatment of the processes gave the best results as they only presented these results in the model evaluation section. I have a few comments here: (1) models with more detailed processes might not provide the best results due to compensating errors in the model. The authors should compare the model performance with the simpler treatment of the processes (e.g. using the Lohmann-Lammel scheme vs. with the ppLFER scheme; using annual emissions vs. seasonal varying emissions).

AR: The influence of sophistication of gas-particle partitioning model, temporal resolution of emissions, and other features/parameterizations, has been tested and discussed in Section 3.1. In Section 3.2 (Model Evaluation), we only evaluated the model results from the *target* experiment to assess the current state of model predictive capability using the most recent knowledge in PAH modeling. On the other hand, Section SVII describes the ranges of model bias obtained from all sensitivity experiments, which is useful to compare model performance from each combination against the *base* configuration simulation (referring to the referee's suggestion). The results vary depending on species, region, and season and it appears difficult to state explicitly if the sophisticated treatment of the processes performs best for all cases. For example: (1) using seasonal emissions brings predictions closer to observations for PHE concentrations, particularly in the northern mid-latitudes; (2) the ppLFER scheme yields smaller Arctic concentrations than the Lohmann-Lammel scheme, leading to higher negative

bias in this region; (3) volatilization would reduce negative bias in BaP concentrations during summer, but may lead to a positive bias in combination with the Lohmann-Lammel scheme.

RC: (2) the model was configured at 2.8 degrees horizontal resolutions thus cannot resolve local gradients when the monitors are not in the remote areas that can represent the average concentrations represented by the grid cells. Are the monitors used in the analyses selected to filter out the non-remote sites?

AR: The referee is correct, we ignored stations that have close proximity to urban and industrial sources, such as all urban sites. Only data from rural background or remote stations were screened and quality checked (following the description in Section SIII).

RC: (3) What's the model performance of BC, total PM and size-resolved PM? What about gaseous pollutants (O3?) The authors didn't mention these in the manuscript. Without these, it is hard to further understand the bias in the model predictions.

AR: Model performance for global distributions of aerosols and gaseous oxidants has been confirmed in previous studies using the EMAC model. The GMXe aerosol microphysics and gas-aerosol partitioning submodel implemented within EMAC has been shown to improve model predictions of various aerosol species, including BC, OM, dust, sea salt, sulfate, ammonium, and nitrate aerosol (Pringle et al., 2010). The simulated values show generally a good agreement with observations for the bulk aerosol species, particularly for BC and OM where at least 90% of modeled values are within a factor of two of the observations. For tropospheric ozone, it has been shown that EMAC reproduces the annual cycle and spatial pattern of observed tropospheric column ozone (Righi et al., 2015). However, the model tends to overestimate the magnitude, in particular over the NH mid-latitudes.

Pringle K. J., Tost H., Message S., Steil B., Giannadaki D., Nenes A., Fountoukis C., Stier P., Vignati E., and Lelieveld, J. (2010) Description and evaluation of GMXe: a new aerosol submodel for global simulations (v1), Geosci. Model Dev. 3, 391–412

Righi M., Eyring V., Gottschaldt K.-D., Klinger C., Frank F., Jöckel P., and Cionni, I (2015) Quantitative evaluation of ozone and selected climate parameters in a set of EMAC simulations, Geosci. Model Dev. 8, 733-768.

RC: (4) the authors have included some discussions on comparing with results with GEOS-Chem. As the resolution, emission inventories, model time spans are all different, this appears to be of less value and can be considered to move to SI. There is a tendency these days to write overly long papers with I am not a big fan of.

AR: We followed the referee's suggestion. In the revised manuscript, the intermodel comparison in Section 3.2.1 has been moved to Supporting Information (see Section SIX and Lines 669-670).

Reply to SC1

In my role as Executive editor of GMD, I would like to bring to your attention our Editorial version 1.1:

http://www.geosci-model-dev.net/8/3487/2015/gmd-8-3487-2015.html

This highlights some requirements of papers published in GMD, which is also available on the GMD website in the 'Manuscript Types' section:
http://www.geoscientific-model-development.net/submission/manuscript_types.html

In particular the following requirements is not fully met in the Discussions paper:
"All papers must include a section, at the end of the paper, entitled 'Code availability'. Here, either instructions for obtaining the code, or the reasons why the code is not available should be clearly stated. It is preferred for the code to be uploaded as a supplement or to be made available at a data repository with an associated DOI (digital object identifier) for the exact model version described in the paper. Alternatively, for established models, there may be an existing means of accessing the code through a particular system. In this case, there must exist a means of permanently accessing the precise model version described in the paper. In some cases, authors may prefer to put models on their own website, or to act as a point of contact for obtaining the code. Given the impermanence of websites and email addresses, this is not encouraged, and authors should consider improving the availability with a more permanent arrangement. After the paper is accepted the model archive should be updated to include a link to the GMD paper."

Last summer the GMD executive Editors and the MESSy consortium agreed to a procedure that meets the GMD requirements as well as the MESSy code development standards. The MESSy website (www.messy-interface.org → License) states (among others) the following: "As the exact code described and used in the paper needs to published, it needs to be ensured, that exactly the code published is part of the next official release (version Y). This requires, that the code is checked in by the developer and approved by the source code administrators before publication, or, to be more precise, before starting the simulations analysed in the publication. In case of doubt, please contact the Consortium Steering Group for advice."

To date, the SVOC code has not been received by the MESSy source code administrators and, consequently, could not be approved for the next official MESSy code release (v2.55). As the permanent availability of the code published in the paper is not yet guaranteed. The paper can not be finally published until the above requirements are met.

AR: The source codes have been received and approved by the Consortium Steering Group to be part of the next official MESSy release of version 2.55. The corresponding author acts as a reference to provide input data and namelist files applied in the study.

Global Simulation of Semivolatile Organic Compounds – Development and Evaluation of the MESSy Submodel SVOC (v1.0)

Mega Octaviani[1]
Holger Tost[2]
Gerhard Lammel[1,3,*]

[1]*Multiphase Chemistry Department, Max Planck Institute for Chemistry, 55128 Mainz, Germany*
[2]*Institute for Atmospheric Physics, Johannes Gutenberg-University Mainz, 55099 Mainz, Germany*
[3]*Research Centre for Toxic Compounds in the Environment, Masaryk University, 62500 Brno, Czech Republic*

*Correspondence to: g.lammel@mpic.de

Submitted to Geoscientific Model Development
Manuscript type: Model description

Abstract

The new submodel SVOC for the Modular Earth Submodel System (MESSy) was developed and applied within the ECHAM5/MESSy Atmospheric Chemistry (EMAC) model to simulate the atmospheric cycling and air-surface exchange processes of semivolatile organic pollutants. Our focus is on four polycyclic aromatic hydrocarbons (PAHs) of largely varying properties. Some new features in input and physics parameterizations of tracers were tested: emission seasonality, the size discretization of particulate-phase tracers, the application of poly-parameter linear free energy relationships in gas-particle partitioning, and re-volatilization from land and sea surfaces. The results indicate that the predicted global distribution of the 3-ring PAH phenanthrene is sensitive to the seasonality of its emissions, followed by the effects from considering re-volatilization from surfaces. The predicted distributions of the 4-ring PAHs fluoranthene and pyrene, and the 5-ring PAH benzo(a)pyrene are found sensitive to the combinations of factors with their synergistic effects being stronger than the direct effects of the individual factors. The model was validated against observations of PAH concentrations and aerosol particulate mass fraction. The annual mean concentrations are simulated to the right order of magnitude for most cases and the model well captures the species and regional variations. However, large underestimation is found ~~in~~ over the ocean. It is found that the particulate mass fraction of the benzo(a)pyrene is well simulated whereas those of other species are lower than observed.

1 Introduction

The atmospheric cycling of semivolatile organic compounds (SOCs) is particularly complex, because of partitioning across phases and air−surface exchange processes, including multihopping (or 'grasshopper effect'; Semeena and Lammel, 2005) and accumulation in ground compartments such as seawater, soil, vegetation, and ice/snow. Many SOCs do resist degradation in environmental compartments, hence, are persistent. In regulation of chemical substances and in international chemicals legislation (e.g. UNEP, 2017), model-based quantifications of the overall environmental residence time (persistence) and the long-range transport potential are requested or encouraged to be applied.

Global and regional distribution and transport of SOCs has been studied using multimedia fate (box) models and chemistry transport models (CTMs) (Scheringer and Wania, 2003). The multimedia models describe the whole or part of the globe as a few zones of homogeneous environmental characteristics (Wania and Mackay, 1999; Mackay, 2010). These models are used as tools to assess the influences of environmental parameters and change on pollutant levels in multiple compartments (Dalla Valle et al., 2007; MacLeod et al., 2005; Lamon et al., 2009). On the other hand, CTMs generally imply the application of three-dimensional Eulerian models coupled with surface and chemistry modules (e.g. Ma et al., 2003; Hansen et al., 2004; Malanichev et al., 2004; Gusev et al., 2005; Semeena et al., 2006; Gong et al., 2007;

Friedman and Selin, 2012; Galarneau et al., 2014; Shrivastava et al., 2017). The addition of a surface module aims to describe air−surface exchange processes and biogeochemical cycles of contaminants whereas a chemistry module describes the changes in air concentrations due to phase partitioning and chemical transformations. Compared to the multimedia models, CTMs have better spatial and temporal resolution but require more computational effort. They are suitable for use to investigate the variability and episodic character of environmental fate and transport. To date, pollutants addressed in model studies were persistent organic pollutants, such as dichlorodiphenyltrichloroethane (DDT), polychlorinated biphenyls (PCBs), hexachlorocyclohexanes (HCHs), polycyclic aromatic hydrocarbons (PAHs), and more recent so-called emerging pollutants (e.g. MacLeod et al., 2011).

The sensitivity of distributions to specific processes of SOC cycling and related input parameters has been the focus of CTM-based studies (Semeena et al., 2006; Sehili and Lammel, 2007; Friedman and Selin, 2012; Galarneau et al., 2014; Thackray et al., 2015). Sehili and Lammel (2007), for instance, suggest that the gas−particle partitioning and particulate-phase oxidation scenarios have significant influences on the long-range atmospheric transport of PAHs. This finding is supported by Friedman and Selin (2012), who, furthermore, concluded that the effects are higher than those of irreversible partitioning and of increased aerosol concentrations.

This study presents the new multicompartment module (submodel) SVOC for the Modular Earth Submodel System (MESSy; Jöckel et al., 2006, 2010). MESSy provides a modular framework for simulations accounting for various degree of complexity and to facilitate a continuous future submodel improvements. The submodel has been applied using the general circulation model ECHAM5 (Roeckner et al., 2003, 2006) as a base model. In connection with the ECHAM5/MESSy (EMAC) model, SVOC encompasses a 3D atmosphere and 2D surface compartments (soil, vegetation, snow, and ocean mixed layer), and considers multicompartment fate and exchange processes, such as emission, phase partitioning, wet and dry deposition of gases and particles, degradation, and air−surface gas exchange, including re-volatilization. ~~The~~ SVOC is developed and intended to be applied for the study of all potentially re-volatilizing and gas-particle partitioning (hence, semivolatile) compounds. Nevertheless, the focus of this submodel development is the global distribution of four PAH species of largely varying properties. PAHs enter the atmospheric environment as by-products of all technological combustion processes (Shen et al., 2013) and of open fires (Gullett et al., 2008). They are ubiquitous pollutants of particular environmental and health concern (WHO, 2003; Laender et al., 2011; Lammel, 2015) and due to their continuous global emissions. Here we describe submodel development, compare the results to observations, and assess the significance of four model features to PAH distributions and fate. These features are the temporal resolution of emissions, the size discretization of particulate-phase tracers (bulk or modal), the choice of the gas−particle partitioning scheme, and re-volatilization from surfaces.

2 Methods

2.1 Model descriptions

The global model applied in this study is the ECHAM/MESSy Atmospheric Chemistry−Climate model (EMAC), a three-dimensional Eulerian model for the simulations of meteorological variables, gaseous, aerosols, clouds, and other climate-related parameters. EMAC combines the general circulation model ECHAM5 (here, version 5.3.02) (Roeckner et al., 2003, 2006) with the Modular Earth Submodel System (MESSy version 2.50; Jöckel et al., 2006, 2010). The atmospheric component ECHAM5 derives four prognostic variables, namely, vorticity, divergence, temperature, and the logarithm of surface pressure in truncated series of spherical harmonics, whereas specific humidity, cloud water, and cloud ice are represented in grid point space. MESSy provides a modular framework to define atmospheric dynamics, chemistry, transport, and radiative transfer processes. For a more detailed description of the EMAC model, evaluation and relevant studies, refer to Jöckel et al. (2006, 2010) and http://www.messy-interface.org. List of MESSy process-based modules, hereinafter submodels, applied in the study are summarized in Table 1.

The new MESSy submodel SVOC for simulating the fate and cycling of SOCs in the global environment is presented. Processes involved in the submodel include gas−particle partitioning, volatilization from the surface, dry and wet depositions, chemical and biotic degradations. These processes are connected to other MESSy submodels. For example, deposition of gas-phase SOCs are calculated by the submodels SCAV and DDEP, aerosol microphysics by GMXe, gas-phase chemistry mechanisms by MECCA, and ocean−air flux exchange by AIRSEA. Figure 1 illustrates the SVOC structure within EMAC system and its interactions with other MESSy submodels. More details on some process parameterizations are given in the following section. A user manual can be found in the Supplement with the list of submodel input and output variables.

Insert Table 1
Insert Figure 1

2.2 Parameterizations of cycling processes in multiple compartments

2.2.1 Representation of SOC in particulate phase

The parameterizations of aerosol microphysical processes for SOCs such as gas-to-particle partitioning and dry and wet deposition depend on the way the particulate phase is represented in the model. Here, there are two approaches employed in the submodel to represent the particulate-phase SOC: 1) it is assumed as a bulk species, or 2) the particle sizes are resolved into n continuous (modal) distributions. The former will be hereinafter referred to as the *bulk* scheme, and the latter referred to as the *modal* scheme. In the *modal* scheme, n is equal to the 7 log-normal modes of the GMXe submodel, four with hydrophilic coating (*ns*:

nucleation soluble, *ks*: Aitken soluble, *as*: accumulation soluble, *cs*: coarse soluble) and three hydrophobic (*ki*: Aitken insoluble, *ai*: accumulation insoluble, *ci*: coarse insoluble) (Pringle et al., 2010). Each mode is treated as an individual tracer.

2.2.2 Partitioning between gas phase and particulate phase

Gas−particle partitioning is assumed to take place when SOC is at equilibrium between the gas and particulate phases. The concentration of the species that is bound to particles (C_{particle}) is calculated with

$$C_{\text{particle}} = \theta \times (C_{\text{particle}} + C_{\text{gas}}) \ , \tag{1}$$

and the particulate mass fraction (θ) is defined as

$$\theta = \frac{C_{\text{particle}}}{C_{\text{particle}} + C_{\text{gas}}} = \frac{K_{\text{p}} \times C_{\text{PM}}}{1 + K_{\text{p}} \times C_{\text{PM}}} = \frac{K_{\text{p}}^{'}}{1 + K_{\text{p}}^{'}} \ , \tag{2}$$

where C_{PM} is the concentration of particulate matter or PM (μg m^{-3}), K_{p} is the temperature-dependent particle−air partition coefficient (m^3 μg^{-1}), and $K_{\text{p}}^{'}$ is the dimensionless K_{p}.

In a model configuration using size-resolved particles (viz. the *modal* scheme), each SOC tracer is introduced in the model as eight different species, seven aerosol particles in *ns*, *ks*, *as*, *cs*, *ki*, *ai*, *ci* modes and one in the gas phase. The particulate fraction of the species in mode i (θ_i) is calculated using Equation 2 with C_{PM_i} and K_{p_i} being the PM mass concentration and aerosol−air partition coefficient in the corresponding mode, respectively. The gaseous concentration C_{gas} is calculated using the sum of K_{p} values across modes, as well as total C_{particle} and C_{PM}:

$$C_{\text{gas}} = \frac{\sum_{i=1}^{7} C_{\text{particle}_i} / \sum_{i=1}^{7} C_{\text{PM}_i}}{\sum_{i=1}^{7} K_{\text{p}_i}} \ . \tag{3}$$

It is noted that this approach may not hold the constraint of mass consistency, and is thus subject to further corrections. For the current study, the effects from this problem are expected to be minimal, given the fact that PAHs in the particulate phase are mainly distributed in the accumulation mode (Lammel et al., 2010, and references therein).

For K_{p} calculation four options of gas−particle partitioning schemes are available in SVOC, they are: (1) a parameterization that is based on adsorption onto aerosol surface (Junge, 1977; Pankow, 1987), (2) absorption into organic matter (Finizio et al., 1997), (3) a combination of two ways of organic matter absorption and black carbon adsorption (Lohmann and Lammel, 2004), and (4) multiple phase of the two-ways sorption system (Goss and Schwarzenbach, 2001; Endo and Goss, 2014; Shahpoury et al., 2016). Two schemes used in this study are described below.

Lohmann–Lammel scheme

The Lohmann−Lammel scheme takes into account an adsorption onto black carbon (BC) surface in addition to absorption into OM (Lohmann and Lammel, 2004). This dual sorption theory empirically calculates K_{p} according to the following relation

$$K_{\mathrm{p}} = 10^{-12} \left(f_{\mathrm{OM}} \, \frac{\gamma_{\mathrm{oct}} \, \mathrm{MW}_{\mathrm{oct}}}{\gamma_{\mathrm{OM}} \, \mathrm{MW}_{\mathrm{OM}} \, \rho_{\mathrm{oct}}} \, K_{\mathrm{oa}} + f_{\mathrm{BC}} \, \frac{a_{\mathrm{atm-BC}}}{a_{\mathrm{soot}} \, \rho_{\mathrm{BC}}} \, K_{\mathrm{sa}} \right) \, , \tag{4}$$

where ρ_{BC} is the density of BC (assumed as 1 kg L^{-1}), ρ_{oct} is the density of octanol (0.82 kg L^{-1} at 20°), K_{sa} is the partition coefficient between diesel soot and air, $a_{\mathrm{atm-BC}}$ is the available surface of atmospheric BC (m^2 g^{-1}), and a_{soot} is the specific surface area of diesel soot (m^2 g^{-1}). The adsorptive properties of diesel soot are selected to represent the atmospheric BC because this material is considered the most significant type of BC in polluted air.

The K_{sa} value is calculated as a function of sub-cooled liquid vapor pressure p_{L}^{0} using an estimate suggested by van Noort (2003),

$$\log K_{\mathrm{sa}} = -0.85 \log p_{\mathrm{L}}^{0} + 8.94 - \log \left(\frac{998}{a_{\mathrm{soot}}} \right) \, , \tag{5}$$

where a_{soot} in the model is set as 18.21 m^2 g^{-1}.

Poly-Parameter Linear Free Energy Relationships (ppLFER) scheme

The concept of poly-parameter linear free energy relationships (ppLFER) for the prediction of equilibrium partition coefficients is introduced by Goss and Schwarzenbach (2001), and its application in environmental chemistry has been reviewed by Endo and Goss (2014). This approach can describe a composite of different types of interactions between gas-phase species and aerosols. In contrast, single-parameter LFERs only correlates the partition coefficient to the sub-cooled liquid vapor pressure or the octanol−air partition coefficient of the species, hence only valid within the group of compounds for which they were developed.

In the study, ppLFER scheme is incorporated into SVOC in which it defines K_p as the sum of individual partition coefficients representing surface adsorption and bulk-phase absorption processes to inorganic and organic aerosols. The formulation of K_p is adopted from Shahpoury et al. (2016) and is described as follows

$$
\begin{aligned}
K_{\mathrm{p}} &= \frac{K_{\mathrm{p}}^{'}}{C_{\mathrm{PM}}} \\
K_{\mathrm{p}}^{'} &= K_{\mathrm{EC}} \times a_{\mathrm{EC}} \times C_{\mathrm{EC}} \times 10^{-6} + \\
&\quad K_{(\mathrm{NH_4})_2\mathrm{SO_4}} \times a_{(\mathrm{NH_4})_2\mathrm{SO_4}} \times C_{(\mathrm{NH_4})_2\mathrm{SO_4}} \times 10^{-6} + \\
&\quad K_{\mathrm{NaCl}} \times a_{\mathrm{NaCl}} \times C_{\mathrm{NaCl}} \times 10^{-6} + \\
&\quad K_{\mathrm{DMSO}} \times \frac{C_{\mathrm{WSOM}}}{\rho_{\mathrm{DMSO}}} \times 10^{-6} + \\
&\quad K_{\mathrm{PU}} \times 0.2 \times C_{\mathrm{WIOM}} \times 10^{-12} + \\
&\quad K_{\mathrm{hexadecane}} \times 0.8 \times \frac{C_{\mathrm{WIOM}}}{\rho_{\mathrm{hexadecane}}} \times 10^{-6}
\end{aligned}
\tag{6}
$$

where K_{EC}, $K_{(\mathrm{NH_4})_2\mathrm{SO_4}}$, and K_{NaCl} are the substance partition (adsorption) coefficients ($\mathrm{m^3_{air}\ m^{-2}_{surface}}$) for elemental−carbon/diesel soot, ammonium sulfate, and sodium chloride aerosol surface−air systems, respectively. K_{DMSO} is the substance partition (absorption) coefficient for dimethyl sulfoxide−air system ($\mathrm{L_{air}\ L^{-1}_{DMSO}}$). K_{PU} is the substance partition (absorption) coefficient for polyurethane−air system ($\mathrm{m^3_{air}\ kg^{-1}_{PU}}$). $K_{\mathrm{hexadecane}}$ is the substance partition (absorption) coefficient for hexadecane−air system ($\mathrm{L_{air}\ L^{-1}_{hexadecane}}$). a_{EC}, $a_{(\mathrm{NH_4})_2\mathrm{SO_4}}$, and a_{NaCl} are the adsorbent specific surface areas: 18.21, 0.1, and 0.1 $\mathrm{m^2_{surface}\ g^{-1}_{adsorbent}}$, respectively. ρ_{DMSO} and $\rho_{\mathrm{hexadecane}}$ are the dimethly sulfoxide and hexadecane densities: 1.1×10^6 and 0.77×10^6 g $\mathrm{m^{-3}}$, respectively. C_{EC}, $C_{(\mathrm{NH_4})_2\mathrm{SO_4}}$, C_{NaCl}, C_{WSOM}, C_{WIOM} are the concentration ($\mu\mathrm{g_{substance}\ m^{-3}_{air}}$) of elemental carbon (here, black carbon), ammonium sulfate, sodium chloride, water-soluble organic matter, and water-insoluble organic matter, respectively.

The ppLFER scheme calculates the sorptive partition coefficient for every aerosol system, as summarized in Table S1. Each ~~of the coefficients~~ coefficient requires information on system parameters (e, s, a, b, v, l), and the constant c, as shown in Table S2. The Abraham solute descriptors (E, S, A, B, V, and L) are substance specific, and for the species selected in this study, refer to Table S6. All the predicted partition constants are adjusted to environmental temperature using the van't Hoff equation

$$
\ln K_{(\mathrm{T})} = \ln K_{(\mathrm{T_0})} - \frac{\Delta \mathrm{H}}{R}\left(\frac{1}{\mathrm{T}} - \frac{1}{\mathrm{T_0}}\right) , \tag{7}
$$

where ΔH is the enthalpy of solvent-air phase transfer in J $\mathrm{mol^{-1}}$. This variable is system specific and calculated by applying the ppLFER equations given in Table S3 and input parameters given in Table S4. The sequence of K_{p} calculation from ppLFER analysis in SVOC is illustrated in Figure S1.

2.2.3 Volatilization

Soil

For soil volatilization, two parameterization schemes are implemented in the SVOC submodel, that is, the Jury scheme (Jury et al., 1983, 1990), and the Smit scheme (Smit et al., 1997). The latter was applied in the study which is based on the volatilization of pesticides from the

surface of fallow soils (Smit et al., 1997). The volatilization occurs upon partitioning over three soil phases (solid, gas, and liquid). The concentration of the chemical in the soil system (kg m^{-3}) is formulated as

$$C_{\text{soil}} = Q \times C_{\text{vapor}} \ , \tag{8}$$

and the capacity factor Q is given by

$$Q = \psi + \varphi K_{\text{wa}} + \rho_{\text{soil}} K_{\text{wa}} K_{\text{sl}} \ , \tag{9}$$

where ψ and φ are the volume fractions of air and moisture, respectively, ρsoil is the soil density, K_{wa} is the water−air partition coefficient where $K_{\text{wa}} = 1/K_{\text{aw}}$, and K_{sl} is the solid−liquid partition coefficient. K_{aw} is calculated based on the Henry's Law constant:

$$K_{\text{aw}} = 1/\left(H \ R \ T\right) \ , \text{ and} \tag{10}$$

$$H = k_{\text{H}}^{\ominus} \times \exp\left[\frac{-\Delta H_{\text{soln}}}{R}\left(\frac{1}{T} - \frac{1}{T_0}\right)\right] \ , \tag{11}$$

where H is the temperature-adjusted Henry coefficient (M atm^{-1}), R is the dry air gas constant (= 8.314 J mol K^{-1}), T is the environment temperature (K), ΔH_{soln} is the enthalpy of dissolution (J mol^{-1}).

K_{sl} can be set equal to the sorption coefficient to soil organic matter K_{om} times the fraction of organic carbon in soil f_{OM_s}. Since K_{om} data is not available, the coefficient for sorption to soil organic carbon K_{oc} was used to estimate K_{sl}:

$$K_{\text{sl}} = 0.56 K_{\text{oc}} f_{\text{OM}_\text{s}} \tag{12}$$

Mackay and Boethling (2000) has suggested a reasonably good regression relationship between K_{oc} and octanol−water partition coefficient K_{ow} for PAHs:

$$\log(K_{\text{oc}}/1000) = 0.823 \log(K_{\text{ow}}/1000) - 0.727 \ . \tag{13}$$

where the factor of 1000 is needed because K_{oc} and K_{ow} are expressed in m^3 kg^{-1} whereas, in the original regression, they used mL g^{-1}.

Once Q is computed, the dimensionless fraction of the chemical in the gas phase F_{gas} is then calculated as

$$F_{\text{gas}} = \frac{\psi}{Q} \ . \tag{14}$$

In the Smit scheme, an empirical relation was established between F_{gas} and cumulative volatilization (CV in % of substance deposit). CV was determined based on field and greenhouse experiments with numerous pesticides at 21 days after application. For normal to moist field conditions, CV is expressed as

$$CV = 71.9 + 11.6 \log(100\ F_{\text{gas}})\ ;\ 6.33 \times 10^{-9} < F_{\text{gas}} \leq 1\ , \tag{15}$$

and for dry field conditions,

$$CV = 42.3 + 9.0 \log(100\ F_{\text{gas}})\ ;\ 0.2 \times 10^{-6} < F_{\text{gas}} \leq 1\ . \tag{16}$$

Vegetation

Smit et al. (1998) derived an equation for the cumulative volatilization CV from plants against vapor pressure P_v (mPa) at seven days after application based on field and climate chamber experiments of pesticide volatilization (Equation 17).

$$CV = 10^{1.528 + 0.466 \log P_v}; P_v \leq 10.3\ . \tag{17}$$

For compounds with P_v above 10.3 mPa, CV is set at 100 % of deposit. Temperature adjustments were made for P_v using the Clausius−Clapeyron equation:

$$\frac{d(\ln P_v)}{dT} = -\frac{\Delta H_{\text{vap}}}{R\ T^2}\ . \tag{18}$$

Snow and glaciers

The parameterization of substance loss by volatilization from snow pack follows Wania (1997) whereby the process is calculated using a consecutive cycle of an equilibrium partitioning among four phases followed by a contaminant loss. The four phases considered are liquid water, organic matter contained in the snowpack, snow pores (air), and an ice−air interface. Fugacity capacity factors for these phases are expressed with the following relations:

air (mol m^{-3} Pa^{-1})	$Z_a = 1/RT$	(19a)
water (mol m^{-3} Pa^{-1})	$Z_l = K_{\text{wa}}/RT = K_{\text{wa}}\ Z_a$	(19b)
organic carbon (mol m^{-3} Pa^{-1})	$Z_o = Z_l\ 0.41\ K'_{\text{ow}}$	(19c)
ice–air interface (mol m^{-2} Pa^{-1})	$z_i = K_{\text{ia}}/RT = K_{\text{ia}}\ Z_a$	(19d)

where R is the dry air gas constant (8.312 J mol^{-1} K^{-1}), T is the air temperature (K), K_{wa} is the water−air partition coefficient (unitless), K'_{ow} is the dimensionless octanol−water partition coefficient, and K_{ia} is the ice surface−air partition coefficient (m). K_{ia} at 20°C is estimated using K_{wa} and water solubility C^s_w (mol m^{-3}),

$$\log K_{\mathrm{ia}}\,(20^{\circ}\mathrm{C}) = -0.769 \log C_w^s - 5.97 + \log K_{\mathrm{wa}}\ , \tag{20}$$

and further extrapolated to other temperatures using enthalpy of condensation of solid (ΔH_{subl} in J mol^{-1}),

$$\log K_{\mathrm{ia}}(T) = \log K_{\mathrm{ia}}\,(20^{\circ}\mathrm{C}) + \frac{0.878\ \Delta H_{\mathrm{subl}}}{2.303\ R}\left(\frac{1}{T} - \frac{1}{293}\right)\ . \tag{21}$$

An equilibrium fugacity f_s is thereby determined by

$$f_s = \frac{M_{\mathrm{sp}}}{Z_a\ v_a + Z_l\ v_l + z_i\ A_{\mathrm{snow}}\ \rho_{\mathrm{mw}} + Z_o v_o}\ , \tag{22}$$

where M_{sp} is the amount of chemical contained in snowpack (the model here applies snow burden of the chemical in kg m^{-2}), v_a, v_l, and v_o is the volume fraction of air, liquid water, and organic matter in snowpack (m^3 m^{-3}). For this study, v_a and v_l values are set to 0.3 and 0.1, respectively, whereas v_o is zero assuming no polluted snow. A_{snow} is the specific snow surface area (m^2 g^{-1}). In Daly and Wania (2004), a value of 0.1 m^2 g^{-1} for A_{snow} was used for snow accumulation period and a linear decrease from 0.1 to 0.01 m^2 g^{-1} was used during the snowmelt period. In SVOC submodel, a value of 0.025 m^2 g^{-1} is adopted for A_{snow} to represent fairly aged snowpack. ρ_{mw} is the density of snowmelt water and here is taken as $7{\times}10^5$ g m^{-3}.

Volatilization rate (kg m^{-2} s^{-1}) is calculated by applying

$$\frac{dM_{\mathrm{sp}}}{dt} = \frac{1}{\frac{1}{U_7\ Z_a} + \frac{1}{U_5\ Z_l\ +\ U_6\ Z_a}} \times \frac{f_s}{h_s}\ , \tag{23}$$

where h_s is the snow depth (m), U_5 is the snow−water phase diffusion mass transfer coefficient (m h^{-1}), U_6 is the snow−air phase diffusion mass transfer coefficient (m h^{-1}), and U_7 is the snow−air boundary layer mass transfer coefficient (m h^{-1}). U_5 and U_6 are calculated from molecular diffusivities in air and water (Equations 24 and 25), whereas a typical value of 5 m h^{-1} is adopted for U_7.

$$U_5 = B_w\ \frac{v_l^{10/3}/(v_a + v_l)^2}{\ln\ 2h_s}\ , \tag{24}$$

$$U_6 = B_a\ \frac{v_a^{10/3}/(v_a + v_l)^2}{\ln\ 2h_s}\ , \tag{25}$$

where B_w and B_a are the molecular diffusivities (m^2 h^{-1}) in water and air respectively. In the model, B_a is derived from the molecular weight (MW) as $B_a = \frac{1.55}{\mathrm{MW}^{0.65}}$ cm^{2}s^{-1}, whereas B_w is set as $1{\times}10^4$ less than B_a, following Schwarzenbach et al. (2005).

Ocean

In the study, the ocean is ~~treated as a two-dimensional compartment (no vertical layer). The flux of chemicals from the ocean to the atmosphere~~ represented as a surface mixed layer of a depth varying spatially and in time without lateral transports. The mixed layer depths were obtained from (de Boyer Montégut et al., 2004). The SOCś volatilization flux from the sea surface is parameterized based on the two-film model of Liss and Slater (1974) and is calculated within the AIRSEA submodel (Pozzer et al., 2006). Note that no ocean and sea-ice dynamics were included in the simulations.

Sorption of SOCs in water to suspended particulate matter (colloidal or sinking detritus) is neglected. Therefore, SOC concentration in surface seawater and, hence, volatilization from sea surface is overestimated, in particular for very lipophilic ($\log K_{\mathrm{ow}} > 6$) substances. This bias is negligible for the substances studied here (PAHs) which are less lipophilic or volatilisation is limited by vapor pressure (e.g., benzo(a)pyrene). Forces from strong winds, dissolved or particulate organics in seawater are transferred to air via sea spray, which adds to particulate OM in air over the ocean (O'Dowd et al., 2008; Qureshi et al., 2009). This process is neglected in the model.

2.2.4 Dry deposition

Dry deposition is simulated using deposition velocities. For gas-phase SOCs, the velocities are calculated by the DDEP submodel (Kerkweg et al., 2006a), whereas particulate-bound SOCs are assumed to deposit at similar rates to other aerosols whose velocities are also computed by DDEP. If the *modal* scheme is selected (see Section 2.2.1), the particle deposition velocity v_d^{SOC} at mode i is equal to the aerosol deposition velocity v_d^{aer} at the respective mode. On the other hand, for the *bulk* scheme, v_d^{SOC} is computed as a weighted average of v_d^{aer} from the four BC modes (*ki*, *ks*, *as*, and *cs*) where the weight is the surface area of BC. This approach is most relevant for PAHs as they are assumed to be predominantly transported by sorption to BC. The above relations are formulated as follows

$$\textit{modal} \text{ scheme:} \qquad v_{d,i}^{\mathrm{SOC}} = v_{d,i}^{\mathrm{aer}} \tag{26a}$$

$$\textit{bulk} \text{ scheme:} \qquad v_{d,\mathrm{bulk}}^{\mathrm{SOC}} = \frac{\sum_{i=1}^{4} S_{\mathrm{BC}_i} \times v_{d,i}^{\mathrm{aer}}}{\sum_{i=1}^{4} S_{\mathrm{BC}_i}} \tag{26b}$$

and the BC surface area per unit volume S_{BC} ($\mathrm{cm}^2\ \mathrm{cm}^{-3}$) is given by

$$S_{\mathrm{BC}_i} = 4\pi \left[r_i \exp\left(\ln^2 \sigma_{g_i}\right) \right]^2 N_i \times \frac{C_{\mathrm{BC}_i}}{C_{\mathrm{aer}_i}} \ , \tag{27}$$

where N_i is the number concentration for mode i (cm^{-3}), r_i is the number radius (cm), σ_{g_i} is the geometric standard deviation, C_{BC_i} is the BC concentration ($\mu\mathrm{g\ m}^{-3}$) in mode i, and C_{aer_i} is the sum of aerosol concentrations in the same mode ($\mu\mathrm{g\ m}^{-3}$).

2.2.5 Wet deposition

Wet deposition is applied to both gas and particulate SOCs. The gaseous fraction is scavenged into cloud and rain droplets according to diffusion limitation, Henry's law equilibrium, and accommodation coefficient, and this process is parameterized and solved empirically in the SCAV submodel (Tost et al., 2006a). Particulate-phase SOCs are scavenged in convective updrafts, rainout and washout, and cloud evaporation, with the rate being proportional to BC wet scavenging; hence the change in SOC concentration is described as

$$\text{\textit{modal} scheme:} \quad \frac{\Delta C_{\mathrm{SOC}_i}}{\Delta t} = \frac{\mu_{\mathrm{SOC}_i}}{\mu_{\mathrm{BC}_i}} \times \frac{\Delta C_{\mathrm{BC}_i}}{\Delta t} \tag{28a}$$

$$\text{\textit{bulk} scheme:} \quad \frac{\Delta C_{\mathrm{SOC}}}{\Delta t} = \frac{\mu_{\mathrm{SOC}}}{\sum_{i=1}^{4} \mu_{\mathrm{BC}_i}} \times \sum_{i=1}^{4} \frac{\Delta C_{\mathrm{BC}_i}}{\Delta t} \tag{28b}$$

where μ is the particle volume mixing ratio ($\mathrm{mol_{SOC/BC}\ mol_{air}^{-1}}$) and Δt is the model time step (s). Note that Equation 28a imposes a restrictive prerequisite, namely, BC and the particle-bound SOC have similar size distributions. When this condition is not met, there is a high possibility of an artificial mass being produced, usually to the largest aerosol mode. To solve this problem, a correction factor is applied and defined as a function of the ratio of positive fluxes to negative fluxes integrated across levels and modes.

2.2.6 Atmospheric degradation

The atmospheric degradation of SOCs in the gas phase as well as within aerosol particles are explicitly treated in SVOC. The gas-phase chemical mechanism is calculated within the MECCA submodel (Sander et al., 2011). SOC gaseous degradation is from photochemical reactions with OH, NO_3, and O_3 radicals which follow a 2^{nd}-order transformation, with the rate constants $k^{(2)}$ obtained from laboratory studies. $k_{\mathrm{OH}}^{(2)}$ value is typically higher, suggesting that oxidation with OH radical is the dominant loss pathway.

Most models do not consider oxidation rate of particulate-phase SOCs as experimental aerosols studied in laboratory cover only a small part of atmospheric relevant aerosols. For PAHs, such as benzo(a)pyrene which stays mostly in the particulate phase, the degradation is more efficient by surface reactions with O_3 (Shiraiwa et al., 2009, and references therein) with the rate depending on the substrate. The SVOC submodel includes degradation process of PAHs on aerosol particles from the O_3 reaction with one assumption, that is, the heterogeneous reaction does not lead to a change in the oxidant concentration. Due to a limited number of kinetic studies of heterogeneous reactions of PAHs, only two species are considered (phenanthrene and benzo(a)pyrene). Nevertheless, the submodel structure provides a relatively straightforward approach to allow more species in the future.

The reaction rate coefficient for particulate-phase PHE with O_3 at aerosol surfaces was derived from laboratory experiments using chemically unspecific model aerosol (silica) with PAH surface coverage of less than a monolayer (Perraudin et al., 2007). To this end, the second

order rate coefficient, $k^{(2)}$, in cm^4 molec^{-1} s^{-1} was derived from the reported PHE decay kinetics, $k^{(2)}_{O_3,het}$ (cm^3 molec^{-1} s^{-1}), as $k^{(2)} = k^{(2)}_{O_3,het} / \left(\frac{S}{V}\right) = (6.2 \pm 4.8) \times 10^{-17}$ cm^4 molec^{-1} s^{-1}, with $\frac{S}{V}$ (cm^{-1}) being the experimental aerosol surface concentration (0.56 ± 0.43 cm^{-1} in Perraudin et al. (2007)Perraudin et al. (2007)). In the submodel, $k^{(2)}_{O_3,het}$ (cm^3 molec^{-1} s^{-1}) is calculated using the ambient aerosol surface concentration. As for BaP, the pseudo-first-order rate coefficient, $k^{(1)}_{O_3,het}$ in s^{-1}, was derived from surface-adsorbed BaP reaction with O_3 on solid organic and salt aerosols following the Langmuir−Hinshelwood mechanism (Kwamena et al., 2004).

2.2.7 Biotic and abiotic degradations

Biotic and abiotic processes in surface compartments contribute to the degradation of chemicals and are strongly dependent on local environmental conditions, for example, nutrient contents, water, temperature, PH, and light. In SVOC, these factors are not explicitly quantified. The degradation is alternatively described as following a first-order decay law (Equation 29), and the rate . The 10 K temperature warming is assumed to double for every 10 K warming the rate of degradation (Equation 30), following recommendations in chemicals risk assessment (European Commission, 2000) and consistent with findings, such as a two-time increase in the growth of hydrocarbon-degrading microbes found in soils (Thibault and Elliott, 1979).

$$\frac{\partial C_{SOC_s}}{\partial t} = -k_{sfc} \times C_{SOC_s} \ , \tag{29}$$

$$k_{sfc(T)} = k_{sfc(T_{ref})} \times 2^{\frac{T-T_{ref}}{10}} \ , \tag{30}$$

where C_{SOC_s} is the substance concentration (kg m^{-3}) in surface compartments (that is, soil, vegetation, or ocean) and k_{sfc} is the first-order decay rate (s^{-1}). T_{ref} is the reference temperature, that is, 298 K for soil and 273 K for ocean. Note that the degradation in vegetation is calculated assuming the same k_{sfc} for the soil compartment.

2.3 Input data

2.3.1 Kinetic and physicochemical properties

The model simulations were performed for four PAH species: phenanthrene (PHE), pyrene (PYR), fluoranthene (FLT), and benzo(a)pyrene (BaP). To simulate the fate and environmental distribution of these species, the model requires some physicochemical properties as summarized in Table S5 of the supplement. These include equilibrium partition coefficients and their related energies of phase transfer. The characteristics from PHE to BaP are indicated by decreasing volatility (as molar mass increases), increasing K_{oa} and K_{ow}, and decreasing water solubility (as C^s_w and Henry's coefficients decrease). The properties also include the second-rate coefficients for homogeneous oxidation with OH, O_3, and NO_3 except for BaP where the gaseous reaction is switched off. Heterogeneous oxidation by O_3 is simulated only

for PHE and BaP. Furthermore, the model also requires compound solute parameters for simulations using the ppLFER gas−particle partitioning scheme (Table S6).

2.3.2 Emissions and other model input

As model input, several emission datasets were employed in the study. Emission estimates for PAHs were obtained from the annual mean inventory of Shen et al. (2013) for the year 2008. They applied regression and technology split methods to construct country-level emissions for six categories (coal, petroleum, natural gas, solid wastes, biomass, and an industrial process category) or six sectors (energy production, industry, transportation, commercial/residential sources, agriculture, and deforestation/wildfire) before further regridding the emissions to a $0.1° \times 0.1°$ grid.

Emissions of aerosol species such as organic carbon (OC), black carbon (BC), mineral dust (DU), and sea salt (SS) were included. For BC and OC, the Representative Concentration Pathway (RCP) 6.0 emission scenario of the IPCC (Intergovernmental Panel on Climate Change) (van Vuuren et al., 2011) was used and accessible via ftp://ftp-ipcc.fz-juelich.de/pub/emissions/gridded_netcdf. Emissions are calculated for anthropogenic, biomass burning, ship, and aircraft. The RCP database provides a seasonality only for the biomass burning and ship emissions. In this study, seasonal scale factors were applied to the anthropogenic emission whereby the seasonality was based upon the monthly variation of the Hemispheric Transport of Air Pollutants (HTAP) v2.2 anthropogenic emission inventory (Janssens-Maenhout et al., 2015). BC emissions from all sectors were assumed to be hydrophobic. For OC, it was assumed to be 65% hydrophilic and 35% hydrophobic upon biomass burning emissions and to be 100% hydrophobic upon anthropogenic and ship emissions. Both OC and BC were emitted at Aitken mode which spans the size range from about 5 to 50 nanometer in diameter. A factor of 1.724 was used to scale the OC emissions to primary organic matter (OM). It is noteworthy that the formation of secondary organic aerosols (SOA) from atmospheric oxidation and condensation of volatile organic compounds (VOCs) were not treated in the simulations. In the model, particulate organic matter is emitted and transported as a bulk aerosol species (OM).

DU and SS emissions were computed online by the ONEMIS submodel (Kerkweg et al., 2006b). DU emission flux is calculated based on wind speed at 10 m altitude and soil parameters (Schulz et al., 1998). The emission of SS particles by bubble bursting is described as wind-speed dependent particle mass and number fluxes at accumulation (50−500 nm) and coarse (>500 nm) modes. In ONEMIS, the fluxes are determined from pre-calculated lookup tables following the Guelle et al. (2001) parameterization. SVOC submodel accounts for OM fraction in the SS mass fluxes (J_{SS}), and the fraction is estimated using a 10 m wind (v_{10})-dependent empirical relationship derived from Figure 2a in Gantt et al. (2011). Equation 31 below is used to calculate the OM mass fluxes, J_{OM}, in kg m^{-2} s^{-1}.

$$J_{\mathrm{OM}} = J_{\mathrm{SS}} \times \frac{1}{2}\left(\frac{0.78}{1+0.03\exp\left(0.48v_{10}\right)} + \frac{0.24}{1+0.05\exp\left(0.38v_{10}\right)}\right) . \quad (31)$$

Emissions of other gases including volatile organic species (SO_2, CO, NH_3, NO, CH_4, and NMHC) were prescribed using the IPCC RCP6.0 dataset (van Vuuren et al., 2011). ~~The model also requires soil propertiesdata (i, e,~~ Global estimates for the soil properties, dry bulk density and organic matter ~~content) and ocean mixed layer depths (de Boyer Montégut et al., 2004)~~ fraction, were obtained from Dunne and Willmott (1996) and Batjes (1996), respectively.

2.4 Observational data

The observation data used for model performance evaluation were collected from several surface monitoring networks: the European Monitoring and Evaluation Programme (EMEP) (Tørseth et al., 2012), the Arctic Monitoring and Assessment Program (AMAP) (Hung et al., 2005), the Great Lakes Integrated Atmospheric Deposition Network (IADN) (IADN, 2014), the Department for Environment, Food & Rural Affairs (DEFRA) UK-AIR (Air Information Resource) program (DEFRA, 2010), and the MONitoring NETwork in the African continent (MONET-Africa) (Klánová et al., 2008). These data were screened and quality controlled according to the description in Supplement SIII. Final stations with reliable monthly data are depicted in Figure 2 wherein shows 3 stations in the Arctic, 19 in the northern mid-latitudes, and 6 in the tropics. The availability of data differs by station, species, and variable of interest; see the site-specific information in Table S10 for total concentration and Table S11 for particulate mass fraction (θ).

Insert Figure 2

The study also compared simulated concentrations in the marine atmosphere to two ship cruise measurement campaigns: 1) on a West to East transect across the tropical Atlantic Ocean (Lohmann et al., 2013), and 2) along the Asian marginal seas, the Indian, and the Pacific Oceans (Liu et al., 2014). The monthly mean modeled values were compared to daily measurements at each sampling points.

2.5 Experiment designs

2.5.1 Model configuration

The model was run on a spectral T42 grid in the horizontal (approximately 2.8° in a lat−lon grid) and 19 unevenly distributed layers in the vertical with the top level at 10 hPa. The vertical layers are discretized using a hybrid coordinate (the lowest level follows the terrain and becomes surfaces of constant pressure in the stratosphere). All simulations were run for a three-year period (i.e., 2007−2009), with a one-year spin-up (i.e., 2006), and nudged toward the European Centre for Medium-range Weather Forecasts (ECMWF) reanalysis data (Dee et al., 2011). Note that the simulation period was selected based on the representative year of

PAH emissions (i.e., 2008) and the availability of reliable observation data (see Supplement SIII).

2.5.2 Sensitivity to the temporal resolution of emissions and process parameterizations

Factor separation analysis (Stein and Alpert, 1993) was used to quantitatively evaluate the contributions to changes in a particular output variable that result from changing components of model input and physics parameterizations. The model sensitivity to four model components (hereinafter, "factors") was tested. The four factors were:

1. Temporal resolution of emissions (hereinafter, *fac1*)
   The PAH emission inventory of Shen et al. (2013) was based on 2008 annual emission totals from all sectors (see Section 2.3.2). The emissions were divided over the year using monthly factors derived from BC anthropogenic emissions. Two sets of simulations were carried out to test the sensitivity of model output to the seasonal profile of emission. The first set used constant emissions throughout the simulations whereas the second set used monthly emission interval.

2. The size-discretization of particulate-phase PAHs (hereinafter, *fac2*)
   The two options for this factor ~~was~~ were tested: *bulk* versus *modal* (Section 2.2.1). Note that with regards to BaP, 95% of the emissions were assumed to be in particulate phase and for the *modal*-scheme scenario, all of the emitted particles are treated as the hydrophobic Aitken (*ki*) tracers.

3. The choice of gas−particle partitioning scheme (hereinafter, *fac3*)
   The present study focuses on the comparison between the Lohmann−Lammel and ppLFER schemes for gas−particle partitioning.

4. The influence of re-volatilization (hereinafter, *fac4*)
   Model runs with volatilization process switched off are compared to those runs which have volatilization switched on.

The factor separation technique is described in Supplement SIV including the equations used to compute the model sensitivity to four factors. A total of 16 (or 2^n) experiments summarized in 3 are necessary to supply the complete solution for the factor analysis. The ABLN experiment is designed to be the *base* simulation (f_0), in which annual emission (A), the *bulk* scheme (B), the Lohmann−Lammel scheme (L), and no re-volatilization (N) were applied. SMPW is referred to as the *target* simulation (f_{1234}) in which the more sophisticated choice of the four features (factors) were tested, i.e., seasonal emissions + *modal* scheme + ppLFER scheme + with re-volatilization. The total (gas + particle) concentration at the lowest model level was selected ~~as the selected output~~ for its higher relevance with all the factors (compared to, e.g., atmospheric burden) and to facilitate direct comparison with observations.

3 Results and discussion

3.1 Sensitivity tests

The analysis of the factor separation results is given below. For each factor, the analysis includes the assessment of direct effects ($\hat{f}_i$) and total interaction effects ($\Sigma\hat{f}_{ij} + \Sigma\hat{f}_{ijk} + \hat{f}_{1234}$) on near-surface PAH concentrations in two seasons, i.e., December−January−February (DJF) and June−July−August (JJA). Figure 4 shows the respective effects for all factors as relative to the seasonal means of the *base* experiment (f_0). A positive value indicates a concentration increase with respect to f_0, whereas a negative indicates a decrease. The spatial distributions of f_0 and f_{1234} seasonal mean concentrations for the four species are shown in Supplement SVI, ~~Figure S4~~ Figures S4 and S5 respectively.

We studied the relative effects in five climate zones (Arctic, northern mid-latitudes, Tropics, southern mid-latitudes, and Antarctica) The global distributions of the relative effects are presented in Figures S6−S13 whereas Figures S14−S21 present the relative interaction effects from the individual combination of factors. In the following, we do not look to interpret concentration responses to each interaction term. Reasons for this are that (1) accounting for all such interactions is complicated given the number of factors and (2) higher-order interactions (combinations of more than two factors) is hard to physically ~~justify~~interpret.

We further investigate the factor effects on model performance by comparing the predicted seasonal mean near-surface concentrations from 16 experiments against observation data in the Arctic and northern mid-latitudes (Supplement SVII).

3.1.1 Effects of seasonality of emissions

Figure 4a shows that using monthly emissions increases PAH concentrations in DJF and decreases the concentrations in JJA over the areas from the middle to high latitudes of NH. This result is expected and is attributed to emissions during the northern winter (summer) ~~are~~ being higher (lower) than annual means and photochemistry being less (more) active. Over the Arctic, the relative changes ($\hat{f}_1/f_0$) in DJF show a median increase of 30% for PHE, PYR and FLT, and 7% for BaP, whereas $\hat{f}_1/f_0$ in JJA are weaker in magnitude for PHE and PYR (−16%) but comparable for FLT (−28%) and BaP (−5%). Accounting for seasonality leads to generally lower bias for PHE, and this effect is more pronounced in middle than in high latitudes (Supplement SVII, Figure S22).

In general, $\hat{f}_1/f_0$ becomes smaller over the northern mid-latitudes by around half. The upper (lower) quartile of $\hat{f}_1/f_0$ in DJF (JJA) indicates about one-quarter areas of the temperate and polar regions experience at least 40% of an increase (decrease), most were located in northeastern Eurasia (see the left panels of Figures S6 and S7). Note $\hat{f}_1/f_0$ over the tropics are small-to-negligible (±1%) mainly due to little variation in emissions from anthropogenic sectors. PAH concentrations may be higher in dry season due to increased amounts of biomass burning, but they are poorly represented in the current inventory. In southern mid- and high-latitudes, the direct effects of emission change are substantially opposite in sign to the

effects seen in the northern latitudes, being negative in DJF (median ranges from −4% to −32%) and positive in JJA (7%−25%).

Insert Figure 4

The total interactions between *fac1* and other factors generally produce opposite signals to $\hat{f}_1$ over middle and high latitudes in the two seasons. This result indicates that the changes in other factors tend to buffer the influence of monthly emission on increasing or decreasing f_0 concentrations. Some exceptions are seen over parts of East Asia in DJF for all species (Figure S6, right panels) and over the Southern Ocean in JJA for BaP (Figure S7, right panels) where the interactions work to reinforce the direct effects. In DJF, the degree of interactions is smaller or comparable to the size of $\hat{f}_1$ for the Arctic and northern mid-latitudes but becomes stronger by at least double for Antarctica. The opposite tendency is seen in JJA but only applies to PYR and FLT. In agreement to $\hat{f}_1$, the interaction effects are less apparent over the tropics. Note that the positive effects in $\hat{f}_{14}$ during local summer tend to be more dominant than the effects in other combinations for PHE, PYR, and FLT (Figures S18-S20). In the simulation, the presence of re-volatilization in summer tends to suppress $\hat{f}_1$ by promoting more gases available for long-range transport, thus implies a negative feedback.

3.1.2 Effects of size-discretization of particulate-phase tracer

The direct effects of the *modal* scheme ($\hat{f}_2$) vary among species (Figure 4c). $\hat{f}_2$ is almost absent for PHE as the species resides almost completely in the gas phase. For PYR and FLT, $\hat{f}_2$ is negative during DJF over northern mid-latitudes ($\hat{f}_2/f_0$ quartiles range from −5% to −30%) and the Arctic (−50% to −75%) whereas it is hardly visible in JJA or over other regions. Further analysis reveals stronger particle deposition results when the aerosol phase is discretized into different modes (not shown). In long-range transport under modal aerosol representation, the aerosols are more associated with larger particles hence particle deposition becomes more effective. The choice of size discretization has only minor effects for atmospheric levels, except for BaP, especially during DJF, for which overestimates are significantly compensated for (Figure S25). Actually, for BaP, the *modal* scheme generally decreases the concentrations in the Arctic (as median, −35% in DJF and −15% during JJA) and increases (approx. 5%) those over mid- and low-latitude landmass (Figures S8d and S9d, left panels).

As is the case for the direct effects, the interaction contributions are peculiar to individual species (Figure 4d). For PHE, the interaction effects in DJF are reflected in negative concentration responses over the Arctic (18%) and positive over Antarctica (7%), in contrast to relatively mild influences over other regions or in JJA. For PYR and FLT, the effects are negative over the Arctic both in DJF (quartiles vary from −20% to −75%) and in JJA (−6% to −120%). It is interesting to note that the interaction between the *modal* and ppLFER schemes has a major influence on the negative signal (Figures S15, S16, S19, S20), suggesting that the

decrease in simulated concentration associated with the change from *bulk* to *modal* could be intensified when the ppLFER scheme is used. In the remaining areas, the interaction effects vary in sign spatially as illustrated in the right panels of Figures S8b,c−S9b,c. Nevertheless, it shows for both species that maximum influences occur over the Southern Ocean in DJF (where the effects may reach two orders of magnitude) and mid-latitude landmass in JJA (more than a factor of five). As for BaP, the median effects are negative (−7% to −30%) in both seasons, although some positive signals are apparent in parts of high latitudes while the tropical oceans bear small synergistic effects. Similar to other species, the degree of interactions are stronger than $\hat{f}_2$ by more than a factor of three for the majority of grid cells (Figures S8d−S9d, right panels). The large fractions of the effects are dominated by two-factor and three-factor combinations related to the interaction with the ppLFER scheme and/or re-volatilization (Figures S17, S21).

3.1.3 Effects of the choice of gas−particle partitioning scheme

Figure 4e shows that the direct effects of the ppLFER scheme ($\hat{f}_3$) show little spatial heterogeneities in both seasons and for all species. The effects are barely important for PHE due to low gas−aerosol partition constant (K_p). $\hat{f}_3$ is positive for PYR and FLT over polar regions and northern mid-latitudes especially in winter when low temperature favors partitioning to aerosols (higher K_p). The median of $\hat{f}_3/f_0$ varies from 1% to 25% with some parts of Antarctica showing an increase larger than 50%. For BaP, the effects are overall negative (by at least −5%) with $\hat{f}_3/f_0$ reflecting a positive north−south gradient (increasing from the Arctic to Antarctica), associated in part with stronger signals over oceans (Figures S10d and S11d, left panels). In particular under the modal size discretization, the choice of gas−particle partitioning scheme has only minor effects for atmospheric levels, except for BaP for which model overestimates are compensated by the choice of the ppLFER scheme (Figure S25). Under the bulk size discretization, the ppLFER scheme tends to enhance some of the overestimate in the Arctic summer (FLT, PYR; Figures S23−S24). The application of ppLFER increases Kp as this module is calculated from not only interaction with BC and OM (as in Lohmann−Lammel scheme) but also with some other aerosol matrices. Higher K_p indicates higher particle mass fraction. For PYR and FLT, this leads to an increase in total atmospheric lifetime as the aerosol phase is not degraded, and can, therefore, be transported over a larger distance. For BaP, the additional particles are subject to depositions and heterogeneous oxidation by ozone, particularly in regions away from sources. The factor influence is notably too small for PHE as oxidations occur in both phases.

The effects from *fac3* interactions vary by region and are relatively stronger than $\hat{f}_3$ (Figure 4f). This finding is common to all species and seasons. The degree of effects is weaker for PHE compared to that for other species. However, the interactions increase polar concentrations in local summer, by 20% to a factor of five, mainly associated with the coupled effect of ppLFER and volatilization ($\hat{f}_{34}$, Figures S14 and S18). For PYR and FLT, there is a high spatial variability over extratropical regions in local summer, as indicated by the interquartile range (distance between the 3rd and 1st quartiles). With regard to synergistic terms, ppLFER

interactions with the *modal* scheme and re-volatilization, in two- or three-factor combinations, are more important than other contributions (Figures S15−S16 and S19−S20). For BaP, the interaction effects show negative signals similar to $\hat{f}_3$, suggesting a positive feedback. The interactions exert a stronger influence on the concentrations of the oceans than on that of land, except in the tropics (Figures S10d and S11d, right panels). The median of relative effects ranges from −1% to a factor of −10, minimum (maximum) in the northern (southern) extratropics. Two second-order interactions likely make major contributions, that is, $\hat{f}_{34}$ which dominates the response over oceans, and $\hat{f}_{23}$ which dominates over land (Figure S17 and S21).

3.1.4 Effects of re-volatilization

The direct effects of re-volatilization ($\hat{f}_4$) are illustrated in Figure 4g. $\hat{f}_4$ is positive in the tropics in both seasons, with the median $\hat{f}_4/f_0$ ranging from 5% to 50%. Intensive re-volatilization in this region would increase net surface fluxes, thereby increasing concentrations. For PHE, positive $\hat{f}_4$ values are more localized over the tropical landmass, whereas negative $\hat{f}_4$ values are predicted over the tropical ocean (Figures S12a and S13a; left panels). The positive (negative) effects over land (ocean) areas are also apparent at higher latitudes during most of the year. This reflects the fact that the negative effects on concentrations over ocean act contrary to the positive effects on net surface fluxes, mainly caused by the non-linear relationships of air−sea gas exchange (deposition and volatilization), air and surface burden, atmospheric oxidation, and emissions. Accounting for re-volatilization compensates for a significant part of underestimates of PHE in the Arctic during summer, but adds to overestimates in mid-latitudes (Figure S22).

For the studied species of mid semivolatility, PYR and FLT, a positive signal is apparent over the high and middle latitudes during local summer in contrast to a negative signal during local winter (Figure 4g). Similar to PHE, the negative signal is confined over oceans (Figures S12b−c and S13b−c; left panels). The summer increases are stronger (20% to a factor of ten) than the winter decreases (−10% to −60%) and the magnitudes are higher in FLT than in PYR. The near-ground concentrations of PYR and FLT are estimated by ≈30−80% in mid-latitudes of which ≈30% are attributable to re-volatilization. In the Arctic, re-volatilization compensates for ≈60% of PYR underestimation (Figure S23) and explains most of ≈60−80% of FLT overestimation (Figure S24). For BaP, $\hat{f}_4$ is positive consistently across regions and seasons ($\hat{f}_4/f_0$ ranges from 20% to a factor of ten), with substantial effects occurring over oceans (Figures S12*d*−S13d; left panels). Accounting for re-volatilization creates some overestimates in the Arctic during summer (Figure S25). It should be noted that the parameterization adopted here to describe volatilization from soils (the Smit scheme) is derived from an experimental study on mid-polar to polar pesticides and there is a need to validate and eventually sophisticate the parameterization to apolar substances.

The interactions generally point toward positive effects for the high-to-medium volatility species (Figure 4h), despite some negative effects present over parts of the southern (northern) oceans in DJF (JJA) (Figures S12−S13; right panels). As for BaP, the effects are uniformly negative, inferring the interactions work in opposition to $\hat{f}_4$. The negative

response is almost entirely caused by the negative $\hat{f}_{34}$, that is, the two-factor interaction between re-volatilization and the ppLFER scheme (Figures S17,S21). Compared to $\hat{f}_4$, the degree of interactions are weaker for PHE, except in polar regions during local summer where the interactions could amplify $\hat{f}_4$. The above implies that $\hat{f}_4$ may point in the right direction regardless of the influences from other factor changes. ~~On the contrary~~In contrast, the degree of interactions is overall comparable to $\hat{f}_4$ for the other species.

3.2 Model evaluation

Model performance using the sophisticated realization of the four features (factors), i.e., Seasonal emission + *Modal* scheme + ppLFER scheme + With re-volatilization (SMPW) is presented below. Two predicted variables are evaluated, that is, total (gas+particle) concentrations and aerosol particulate mass fraction at the lowest model level. The metrics applied is listed in Supplement SV.

3.2.1 Near-surface air concentration

Comparison to land monitoring stations

Central tendency. Table 2 shows statistical indices for near-surface concentrations of atmospheric PAHs from observations and simulations and their comparisons, averaged across stations in the Arctic, northern mid-latitudes, and the tropics. We can see that mean observed concentrations are higher for PHE and smaller for BaP over all regions. Furthermore, the Arctic concentrations are lower than those in the northern mid-latitudes by a factor of around 20 and those in the tropics by approx. two orders of magnitude. The model captures well these species and regional variations, but the magnitudes are both under- and over-estimated. In the Arctic, it underestimates PHE (MB = -0.060 ng m^{-3}) and BaP (MB = -0.006 ng m^{-3}) concentrations but slightly overestimates PYR (MB = 0.001 ng m^{-3}) and FLT (MB = 0.04 ng m^{-3}). In the NH mid-latitudes, the model overestimates the three species predominantly ~~occur~~ occurring in the gas phase (MB = 0.077$-$0.867 ng m^{-3}) but underestimates BaP (MB = -0.58 ng m^{-3}). Negative bias is seen in the tropics for three PAHs (MB = -3.443 to -6.851 ng m^{-3}). Nevertheless, the comparison of model and observations at individual monitoring station can be different from the regional mean statistics, as described in Supplement SVIII. Comparing all four PAHs, a larger degree of bias is found for BaP which increases from the northern mid-latitudes (NMB = -0.58, NMBF = -1.40, FAC2 = 0.31, FAC10 = 0.79) to the Arctic (NMB = -0.92, NMBF = -12.17, FAC2 = 0.17, FAC10 = 0.33).

Insert Table 2

Dispersion of monthly concentrations. In the following, the coefficient of variation (CoV) is used to compare the dispersion of concentrations among species of different ranges. CoV

was calculated by dividing standard deviation (SD) of all data points by its mean value ($\overline{x}$). The observations show high variability (CoV $>$ 1) with CoV ranging between 1.12 and 2.14. The simulated concentrations appear to be less dispersed than the observations (CoV = 0.78−1.93) except for the Arctic PHE and PYR concentrations. The degree of underestimation is larger in the tropics with CoV being 30%−50% smaller than the observations. Furthermore, correlations between predicted and observed concentrations are weaker than those in other regions where r varies between 0.29−0.63 (the model reproduces 8%−40% of the variance in observed concentrations). Comparing the four species, the simulated BaP shows greater underpredictions of the variability where CoV values are less than half of those observed and correlations are less than 0.2 (accounting not over than 4% of observed variance). Higher variability in BaP measurements (than in model results) can be influenced by strongly varying emissions in source regions that are not reflected in emission inventory (Matthias et al., 2009).

Seasonal variation. Figure 5 compares simulated and observed seasonal cycle of average concentrations for different species and regions. The observed mean concentrations are largest in winter and lowest during summer because of less emission and the strong presence of OH for oxidation. The winter maximum to summer minimum ratio (amplitude) is more pronounced (by more than a factor of two) in the Arctic than that in the NH mid-latitudes. The seasonality between model and observations is in ~~a~~ qualitative agreement, particularly over the Arctic (except in summer) and mid-latitudes. In the Arctic, the model overestimates the seasonal amplitude of PHE and BaP and underestimates their mean concentrations. The contrast is seen for PYR and FLT. FLT concentration is overestimated by up to a factor of three in summer while PYR is quite well predicted. In the NH mid-latitudes, the model underestimates the amplitude but overestimates the concentrations of PHE, PYR, and FLT (by typically a factor of two), whereas a systematic negative bias is found for BaP. In the tropics, both the amplitude and magnitude are too low in the model (for magnitude, by a factor of 2−5).

Additional findings are discussed in Supplement SIX related to the comparison between EMAC model results and those from other global PAH modeling studies.

Insert Figure 5

~~*Intermodel comparison.* A comparison of simulated PAH concentrations from the new EMAC model (with SVOC submodel) for the year 2007−2009 and from GEOS-Chem model for 2005−2009 (Friedman and Selin, 2012) revealed that both models overall overestimate observed PHE and PYR over mid-latitudes whereas the Arctic concentrations for both species are underestimated by EMAC but overestimated by GEOS-Chem in winter. The discrepancies are more likely to be caused by different emission inventory and by high spatial variability in the emissions which results in changes in PAH concentrations on scales not captured by both GCMs with a grid spacing of >100 km. It is also noteworthy that the simulation carried out with GEOS-Chem differs in complexity to EMAC , that is, the model neglected volatilization and seasonal variation in emissions and applied a dual~~

~~BC adsorption and OM absorption gas–particle partitioning. Nevertheless, both models systematically underestimate the BaP concentrations over all regions, reflecting a difficulty in modeling the behavior of this species. Model bias is usually larger for the Arctic sites than for the mid-latitude sites and the agreement with observations is more satisfactory in summer. BaP underestimation in remote regions has also been reported in other global modeling studies (Schili and Lammel, 2007; Shrivastava et al., 2017). Despite uncertainties in the emissions, which seasonality has been taken into account in our simulations, this finding suggests that current models underestimate the role of temperature for the long-range transport of BaP. A GEOS-Chem configuration which neglected heterogeneous oxidations for BaP yielded predicted concentrations higher than measurements over NH mid-latitudes but rather in a good agreement over the Arctic (Friedman and Selin, 2012), suggesting a strong dependence of BaP long-range transport on the temperature sensitivity of particulate-phase oxidation. Similarly, agreement/overprediction of BaP was found using ECHAM5/HAM model (Lammel et al., 2009) when setting $k^{(2)}_{O_3,het}$ to zero (BAPOB scenario; agreement for the Zeppelin station, overestimation for the Alert station). In addition, the latest global BaP modeling study carried out with CAM5 model (Shrivastava et al., 2017) also found that temperature and humidity are important factors to affect heterogeneous oxidation kinetics of BaP and influence the long-range transport. Their default simulation underestimates observed BaP concentrations by approximately 77% whereas the predictions improved when the model assumed that BaP underwent a complete shielding by highly viscous organic aerosols under cool/dry conditions. It is important to understand further the effect of the variation of temperature and humidity on reactive rate constants of the heterogeneous oxidations during the long-range transport. This topic is discussed in details in Mu et al. (2018).~~

Comparison to ship cruise measurements

Measurements of PHE, PYR, and FLT concentrations over the Atlantic Ocean were taken during a cruise in July 2009 (Lohmann et al., 2013). Figure 6 shows the ship sample concentrations overlaying the simulated PAH concentrations. Sample arithmetic (geometric) means during the whole cruise transect are 322 (209), 95 (88), and 128 (111) pg m^{-3} for PHE, PYR, and FLT respectively. The model poorly reproduces the remote marine environments and overall underestimates the observations, except at 3 locations along the North American coast. The simulated means across sampling positions are 23 (7), 20 (3), and 39 (2) pg m^{-3} respectively and the underestimation ranges from a factor of 2 to 1000. The degree of bias is most apparent over the tropical South Atlantic at latitude bands 5°S-15°S.

As reported in Liu et al. (2014), the measured concentrations of BaP over the Asian marginal seas, the Indian Ocean, the South and North Pacific Oceans are 131 (45), 14 (3), 9 (2), and 8 (3) pg m^{-3}, respectively, for the arithmetic (geometric) means of all samples. Similar to other species, the model also underestimates the BaP concentrations with mean values being 75 (15), 4 (0.05), 0.09 (0.03), and 0.2 (0.06) pg m^{-3}, respectively. The discrepancy appears relatively smaller over the Asian marginal seas as compared to other locations (Figure 7). A substantial degree of bias is seen over the Indian Ocean covering approximately the area

bounded by 70°E−90°E and 10°S−30°S, with simulated values being more than two orders of magnitude smaller than the observed.

Insert Figure 6

Insert Figure 7

The model tendency to underestimate the marine air concentrations may likely be due to several factors: (a) The grid resolution is not sufficient to reproduce fine-scale processes at the grid points close to shipping tracks; (b) Great uncertainties associated with the air−sea gas exchange parameterizations still exist, most notably in the estimation of gas transfer velocity; (c) The global inventory (Shen et al., 2013) may significantly underestimate emissions from ocean shipping and ~~do~~ does not well characterize the spatial and temporal variability of biomass burning plumes as another potential ~~origins of~~ point of origin of pollutans in the marine air (Nizzetto et al., 2008); (d) PAH concentration over remote oceans is controlled by atmospheric components (e.g., temperature, wind speed, boundary layer height, photochemical degradation) and the dynamical and biogeochemical components of the ocean. However, the ocean components have not been covered in the simulation; (e) The particulate-bound PAHs may undergo too fast heterogeneous oxidation (most relevant for BaP), leading to short atmospheric lifetimes and weaker long-range transport. BaP, mostly stays in the particulate phase, presumably also in seawater, therefore, may be somewhat underestimated due to the neglect of sea-spray driven aerosol suspension.

3.2.1 Particulate mass fraction

Measurements of particulate mass fraction (θ) were available only from E3 station in Europe and IADN stations (I1-I7) in North America (see Table S11). Table 3 presents summary statistics on monthly mean θ from observations and simulations including some performance metrics. The observed mean θ is smaller for PHE (0.051 ± 0.035) and higher for BaP (0.949 ± 0.067). This result is expected as volatility decreases (hence θ increases) from (lighter) PHE to (heavier) BaP. The θ values for PYR and FLT are larger by over five times than those for PHE and lower by around one-third than those for BaP. The model reproduces well the distinct differences among species but underestimates the observed θ for PHE, PYR and FLT. The degree of negative bias is relatively large in PHE (NMB = −0.910 and NMBF = −10.145), whereas for the isomer pair of PYR and FLT, the model exhibits a similar performance with a slight improvement in PYR (NMB = −0.410 and NMBF = −0.694). With regard to BaP, there is a satisfactorily small bias (MB = 0.015, RMSE = 0.074, NMB = 0.016, and NMBF = 0.016) although the observed and simulated values have a very weak correlation ($r = 0.03$).

Figure 8 shows the seasonal mean θ averaged over three years for all PAHs. Observations show that θ for BaP varies less than those for 3−4 ring PAHs. Although the model adequately reproduces this feature as well as seasonal variation of individual species, the simulated θ of PHE, PYR, and FLT are generally lower than the observations (except for PYR in winter).

For BaP, differences between model and observations are less than 10% in all months. The SVOC submodel describes the gas−particle partitioning of atmospheric SOCs as a function of temperature and aerosol phase composition. The underestimation might be related to the fact that the submodel assumes the particle to be fully in equilibrium with the gas phase at all times. It neglects kinetic limitations of molecular diffusivity that could lead to the trapping of particles inside viscous (or semisolid) organic aerosol coating. This shielding effect increases equilibration times of the particles, thereby reducing part of θ from the mass available for gas−particle partitioning. Deviations from measurements can also be partly attributed to the locations of some stations that are within, or close to, residential and industrial area (namely, I4, I6, and I7) where the scale and gradient in anthropogenic emissions are not resolved by the model grid resolution nor represented by the emission inventory.

Insert Table 3
Insert Figure 8

4 Summary and conclusions

The submodel SVOC has been developed and operated within the EMAC model for the application to global distribution and environmental fate of SOCs. In this first development, the focus was set on the predictions of four PAH species: phenanthrene (PHE), pyrene (PYR), fluoranthene (FLT), and benzo(a)pyrene (BaP). Multicompartmental fate and air−surface exchange processes were included in SVOC. Some novel features in PAH modeling were tested, including seasonality in emissions, the *modal* scheme for particulate-phase tracer representation, the ppLFER scheme for gas−particle partitioning, and re-volatilization from surfaces. The results indicate that using seasonal emission compensates for model biases in the predictions of more volatile species (PHE) whereas the effects of the *modal* and ppLFER schemes are of less significance. Re-volatilization increases the near-ground concentrations in air, which is found most significant for species of mid semivolatility (PYR and FLT). Hereby attribution of model response to individual features (factors) is blurred by the non-linear interactions between two and more factors. The effects of these interactions are found to both reinforce (positive feedback) and suppress (hence, negative feedback) the effects of the individual factors.

For near-surface concentrations, model bias varies by region and/or species, being negative (positive) in the Arctic within typically a factor of 2−13 (6% to a factor of two) for PHE and BaP (PYR and FLT), positive in the northern mid-latitudes for PHE, PYR, and FLT by up to a factor of three, negative in the Tropics (by a factor of 2−3) and largely over ocean up to a factor of three orders of magnitude. The model adequately reproduces the seasonal variation of the particulate mass fraction (θ), but underestimates θ for high-to-medium volatility PAHs. This might be related to a systematic underestimation of OC by the model, which neglects secondary organic aerosols (SOA). The latter may cause significant underestimation of the overall atmospheric aerosol burden and θ of SOCs, in particular over ocean. Since recently

a MESSy submodel, ORACLE, dedicated to the simulations of SOA (Tsimpidi et al., 2014) based on lumping organic species in volatility bins is available. It should be included in future SOC simulations using EMAC.

Moreover, SVOC implicit assumption of instantaneous gas−particle equilibrium may cause both over- and underestimates of θ, as inter-phase mass transfer my be kinetically limited to gaseous sources (hence, overestimate of θ) or within the particle bulk (hence, underestimate θ), as the PAHs may become trapped within particles during transport (Friedman et al., 2014; Zelenyuk et al., 2012; Mu et al., 2018). For multidecadal studies, the coupling of a 3D ocean model (coupled with a marine biogeochemistry module) would be needed since the present model application does not allow for horizontal and vertical transports in the deep ocean. For the same reason, contaminant remobilization within deep soil layers should also be introduced. To this end, a multi-layer (3D) soil compartment would be needed to replace the 2D soil compartment used here.

Code availability

SVOC submodel presented here has been based on the Modular Earth Submodel System (MESSy) version 2.50 and the global atmospheric model ECHAM version 5.3.02. MESSy is continuously further developed and applied by a consortium of institutions. The usage of MESSy and access to the source code is licensed to all affiliates of institutions which are members of the MESSy Consortium. Institutions can be a member of the MESSy Consortium by signing the MESSy Memorandum of Understanding. More information can be found on the MESSy Consortium website (http://www.messy-interface.org). The SVOC submodel will be incorporated into the next released version of the ECHAM/MESSy (EMAC) model (v2.55) and will therefore be made publicly available (with respect to the EMAC license regulations).

Author contributions

M.O. and G.L. conceived the study and designed the experiments. M.O. developed the SVOC submodel with input from all co-authors. M.O. performed model simulations and data analyses. M.O and G.L discussed the results. M.O. wrote the manuscript with contributions from all co-authors.

Acknowledgements

This study was supported by the Max Planck Institute for Chemistry. We thank the MESSy community and MESSy submodel developers for providing technical support. The model simulation was performed at the Max Planck Computing and Data Facility (MPCDF), Garching.

References

Batjes, N.: Total carbon and nitrogen in the soils of the world, Europ. J. Soil Sci., 47, 151–163, doi:10.1111/j.1365-2389.1996.tb01386.x, URL https://onlinelibrary.wiley.com/doi/abs/10.1111/j.1365-2389.1996.tb01386.x, 1996.

Dalla Valle, M., Codato, E., and Marcomini, A.: Climate change influence on POPs distribution and fate: A case study, Chemosphere, 67, 1287–1295, doi:10.1016/j.chemosphere.2006.12.028, URL http://www.sciencedirect.com/science/article/pii/S0045653506017541, 2007.

Daly, G. L. and Wania, F.: Simulating the influence of snow on the fate of organic compounds, Environ. Sci. Technol., 38, 4176–4186, doi:10.1021/es035105r, URL http://pubs.acs.org/doi/pdfplus/10.1021/es035105r, 2004.

de Boyer Montégut, C., Madec, G., Fischer, A. S., Lazar, A., and Iudicone, D.: Mixed layer depth over the global ocean: An examination of profile data and a profile-based climatology, J. Geophys. Res. (Oceans), 109, C12 003, doi:10.1029/2004JC002378, URL http://onlinelibrary.wiley.com/doi/10.1029/2004JC002378/abstract, 2004.

Dee, D. P., Uppala, S. M., Simmons, A. J., Berrisford, P., Poli, P., Kobayashi, S., Andrae, U., Balmaseda, M. A., Balsamo, G., Bauer, P., Bechtold, P., Beljaars, A. C. M., van de Berg, L., Bidlot, J., Bormann, N., Delsol, C., Dragani, R., Fuentes, M., Geer, A. J., Haimberger, L., Healy, S. B., Hersbach, H., Hólm, E. V., Isaksen, L., Kållberg, P., Köhler, M., Matricardi, M., McNally, A. P., Monge-Sanz, B. M., Morcrette, J.-J., Park, B.-K., Peubey, C., de Rosnay, P., Tavolato, C., Thépaut, J.-N., and Vitart, F.: The ERA−Interim reanalysis: configuration and performance of the data assimilation system, Q. J. Roy. Meteor. Soc., 137, 553–597, doi:10.1002/qj.828, URL https://rmets.onlinelibrary.wiley.com/doi/pdf/10.1002/qj.828, 2011.

DEFRA: UK Department of Environment, Food and Rural Affairs. Polycyclic Aromatic Hydrocarbons (PAH) data, URL https://uk-air.defra.gov.uk/data/pah-data, 2010.

Dunne, K. A. and Willmott, C. J.: Global distribution of plant-extractable water capacity of soil, Int. J. Climatol., 16, 841–859, doi:10.1002/(SICI)1097-0088(199608)16:8<841::AID-JOC60>3.0.CO;2-8, URL https://rmets.onlinelibrary.wiley.com/doi/10.1002/%28SICI%291097-0088%28199608%2916%3A8%3C841%3A%3AAID-JOC60%3E3.0.CO%3B2-8#, 1996.

Endo, S. and Goss, K.-U.: Applications of polyparameter linear free energy relationships in environmental chemistry, Environ. Sci. Technol., 48, 12 477–12 491, doi:10.1021/es503369t, URL http://pubs.acs.org/doi/abs/10.1021/es503369t, 2014.

European Commission: Guidance document on persistence in soil, Technical Report 9188/VI/97 in relation to Council Directive No. 97/57/EC, EC Directorate General for Agriculture, 2000.

Finizio, A., Mackay, D., Bidleman, T., and Harner, T.: Octanol−air partition coefficient as a predictor of partitioning of semi-volatile organic chemicals to aerosols, Atmos. Environ., 31, 2289–2296, doi:10.1016/S1352-2310(97)00013-7, URL http://www.sciencedirect.com/science/article/pii/S1352231097000137, 1997.

Friedman, C. L. and Selin, N. E.: Long-range atmospheric transport of polycyclic aromatic hydrocarbons: global 3-D model analysis including evaluation of Arctic sources, Environ. Sci. Technol., 46, 9501–9510, doi:10.1021/es301904d, URL http://pubs.acs.org/doi/pdfplus/10.1021/es301904d, 2012.

Friedman, C. L., Pierce, J. R., and Selin, N. E.: Assessing the influence of secondary organic versus primary carbonaceous aerosols on long-range atmospheric polycyclic aromatic hydrocarbon transport,

Environ. Sci. Technol., 48, 3293–3302, doi:10.1021/es405219r, URL http://pubs.acs.org/doi/pdfplus/10.1021/es405219r, 2014.

Galarneau, E., Makar, P. A., Zheng, Q., Narayan, J., Zhang, J., Moran, M. D., Bari, M. A., Pathela, S., Chen, A., and Chlumsky, R.: PAH concentrations simulated with the AURAMS-PAH chemical transport model over Canada and the USA, Atmos. Chem. Phys., 14, 4065–4077, doi:10.5194/acp-14-4065-2014, URL http://www.atmos-chem-phys.net/14/4065/2014/, 2014.

Gantt, B., Meskhidze, N., Facchini, M. C., Rinaldi, M., Ceburnis, D., and O'Dowd, C. D.: Wind speed dependent size-resolved parameterization for the organic mass fraction of sea spray aerosol, Atmos. Chem. Phys., 11, 8777–8790, doi:10.5194/acp-11-8777-2011, URL http://www.atmos-chem-phys.net/11/8777/2011/, 2011.

Gong, S. L., Huang, P., Zhao, T. L., Sahsuvar, L., Barrie, L. A., Kaminski, J. W., Li, Y. F., and Niu, T.: GEM/POPs: a global 3-D dynamic model for semi-volatile persistent organic pollutants — Part 1: Model description and evaluations of air concentrations, Atmos. Chem. Phys. Discuss., 7, 4001–4013, doi:10.5194/acp-7-4001-2007, URL http://www.atmos-chem-phys.net/7/4001/2007/, 2007.

Goss, K.-U. and Schwarzenbach, R. P.: Linear free energy relationships used to evaluate equilibrium partitioning of organic compounds, Environ. Sci. Technol., 35, 1–9, doi:10.1021/es000996d, URL https://pubs.acs.org/doi/pdfplus/10.1021/es000996d, 2001.

Guelle, W., Schulz, M., Balkanski, Y., and Dentener, F.: Influence of the source formulation on modeling the atmospheric global distribution of sea salt aerosol, J. Geophys. Res. (Atmos.), 106, 27 509–27 524, doi:10.1029/2001JD900249, URL http://onlinelibrary.wiley.com/doi/10.1029/2001JD900249/abstract, 2001.

Gullett, B., Touati, A., and Oudejans, L.: PCDD/F and aromatic emissions from simulated forest and grassland fires, Atmos. Environ., 42, 7997–8006, doi:10.1016/j.atmosenv.2008.06.046, URL http://www.sciencedirect.com/science/article/pii/S1352231008006006, 2008.

Gusev, A., Mantseva, E., Shatalov, V., and B., S.: Regional Multicompartment Model MSCE-POP, EMEP/MSC-E Technical Report 5, 2005.

Hansen, K. M., Christensen, J. H., Brandt, J., Frohn, L. M., and Geels, C.: Modelling atmospheric transport of α-hexachlorocyclohexane in the Northern Hemisphere with a 3-D dynamical model: DEHM-POP, Atmos. Chem. Phys., 4, 1125–1137, doi:10.5194/acp-4-1125-2004, URL http://www.atmos-chem-phys.net/4/1125/2004/, 2004.

Hung, H., Blanchard, P., Halsall, C. J., Bidleman, T. F., Stern, G. A., Fellin, P., Muir, D. C. G., Barrie, L. A., Jantunen, L. M., Helm, P. A., Ma, J., and Konoplev, A.: Temporal and spatial variabilities of atmospheric polychlorinated biphenyls (PCBs), organochlorine (OC) pesticides and polycyclic aromatic hydrocarbons (PAHs) in the Canadian Arctic: Results from a decade of monitoring, Sci. Total Environ., 342, 119–144, doi:10.1016/j.scitotenv.2004.12.058, URL http://www.sciencedirect.com/science/article/pii/S0048969704008411, 2005.

IADN: Great Lakes Integrated Atmospheric Deposition Network, URL http://ec.gc.ca/data_donnees/STB-AQRD/Toxics/IADN, 2014.

Janssens-Maenhout, G., Crippa, M., Guizzardi, D., Dentener, F., Muntean, M., Pouliot, G., Keating, T., Zhang, Q., Kurokawa, J., Wankmüller, R., Denier van der Gon, H., Kuenen, J. J. P., Klimont, Z., Frost, G., Darras, S., Koffi, B., and Li, M.: HTAP_v2.2: A mosaic of regional and global emission grid maps for 2008 and 2010 to study hemispheric transport of air pollution, Atmos. Chem. Phys., 15, 11 411–11 432, doi:10.5194/acp-15-11411-2015, URL http://www.atmos-chem-phys.net/15/11411/2015/, 2015.

Jöckel, P., Tost, H., Pozzer, A., Brühl, C., Buchholz, J., Ganzeveld, L., Hoor, P., Kerkweg, A., Lawrence, M., nbsp, G, Sander, R., Steil, B., Stiller, G., Tanarhte, M., Taraborrelli, D., van Aardenne, J., and Lelieveld, J.: The atmospheric chemistry general circulation model ECHAM5/MESSy1: Consistent simulation of ozone from the surface to the mesosphere, Atmos. Chem. Phys., 6, 5067–5104, doi:10.5194/acp-6-5067-2006, URL http://www.atmos-chem-phys.net/6/5067/2006/, 2006.

Jöckel, P., Kerkweg, A., Pozzer, A., Sander, R., Tost, H., Riede, H., Baumgaertner, A., Gromov, S., and Kern, B.: Development cycle 2 of the Modular Earth Submodel System (MESSy2), Geosci. Model Dev., 3, 717–752, doi:10.5194/gmd-3-717-2010, URL http://www.geosci-model-dev.net/3/717/2010/, 2010.

Junge, C.: Basic considerations about trace constituents in the atmosphere as related to the fate of global pollutants, pp. 7–26, John Wiley & Sons, New York, 1977.

Jury, W. A., Spencer, W. F., and Farmer, W. J.: Behavior assessment model for trace organics in soil: I. Model description, J. Environ. Qual., 12, 558–564, doi:10.2134/jeq1983.00472425001200040025x, URL https://www.soils.org/publications/jeq/abstracts/12/4/558, 1983.

Jury, W. A., Russo, D., Streile, G., and El Abd, H.: Evaluation of volatilization by organic chemicals residing below the soil surface, Water Resour. Res., 26, 13–20, doi:10.1029/WR026i001p00013, URL http://onlinelibrary.wiley.com/doi/10.1029/WR026i001p00013/pdf, 1990.

Kerkweg, A., Buchholz, J., Ganzeveld, L., Pozzer, A., Tost, H., and Jöckel, P.: Technical Note: An implementation of the dry removal processes DRY DEPosition and SEDImentation in the Modular Earth Submodel System (MESSy), Atmos. Chem. Phys., 6, 4617–4632, doi:10.5194/acp-6-4617-2006, URL http://www.atmos-chem-phys.net/6/4617/2006/, 2006a.

Kerkweg, A., Sander, R., Tost, H., and Jöckel, P.: Technical Note: Implementation of prescribed (OFFLEM), calculated (ONLEM), and pseudo-emissions (TNUDGE) of chemical species in the Modular Earth Submodel System (MESSy), Atmos. Chem. Phys., 6, 3603–3609, doi:10.5194/acp-6-3603-2006, URL http://www.atmos-chem-phys.net/6/3603/2006/, 2006b.

Klánová, J., Cupr, P., Holoubek, I., Boruvková, J., Přibylová, P., Kareš, R., Kohoutek, J., Dvorská, A., Tomšej, T., and Ocelka, T.: Application of passive sampler for monitoring of POPs in ambient air. VI. Pilot study for development of the monitoring network in the African continent (MONET-AFRICA 2008), RECETOX_TOCOEN 343, RECETOX MU Brno, Czech Republic, 2008.

Kwamena, N.-O. A., Thornton, J. A., and Abbatt, J. P. D.: Kinetics of surface-bound benzo[a]pyrene and ozone on solid organic and salt aerosols, J. Phys. Chem. A, 108, 11 626–11 634, doi:10.1021/jp046161x, URL http://pubs.acs.org/doi/abs/10.1021/jp046161x, 2004.

Laender, F. D., Hammer, J., Hendriks, A. J., Soetaert, K., and Janssen, C. R.: Combining monitoring data and modeling identifies PAHs as emerging contaminants in the Arctic, Environ. Sci. Technol., 45, 9024–9029, doi:10.1021/es202423f, URL https://pubs.acs.org/doi/pdfplus/10.1021/es202423f, 2011.

Lammel, G.: Polycyclic aromatic compounds in the atmosphere — A review identifying research needs, Polycycl. Aromat. Comp., pp. 1–14, doi:10.1080/10406638.2014.931870, URL http://www.tandfonline.com/doi/abs/10.1080/10406638.2014.931870, 2015.

Lammel, G., Sehili, A. M., Bond, T. C., Feichter, J., and Grassl, H.: Gas/particle partitioning and global distribution of polycyclic aromatic hydrocarbons — A modelling approach, Chemosphere, 76, 98–106, doi:10.1016/j.chemosphere.2009.02.017, URL http://www.sciencedirect.com/science/article/pii/S0045653509001738, 2009.

Lammel, G., Klánová, J., Ilić, P., Kohoutek, J., Gasić, B., Kovacić, I., and Škrdlíková, L.: Polycyclic aromatic hydrocarbons in air on small spatial and temporal scales — II. Mass size distributions and gas−particle partitioning, Atmos. Environ., 44, 5022–5027, doi:10.1016/j.atmosenv.2010.08.001, URL http://www.sciencedirect.com/science/article/pii/S1352231010006540, 2010.

Lamon, L., Dalla Valle, M., Critto, A., and Marcomini, A.: Introducing an integrated climate change perspective in POPs modelling, monitoring and regulation, Environ. Pollut., 157, 1971–1980, doi:10.1016/j.envpol.2009.02.016, URL http://www.sciencedirect.com/science/article/pii/S0269749109000815, 2009.

Landgraf, J. and Crutzen, P. J.: An efficient method for online calculations of photolysis and heating rates, J. Atmos. Sci., 55, 863–878, doi:10.1175/1520-0469(1998)055<0863:AEMFOC>2.0.CO;2, URL https://journals.ametsoc.org/doi/abs/10.1175/1520-0469%281998%29055%3C0863%3AAEMFOC%3E2.0.CO%3B2, 1998.

Lauer, A., Eyring, V., Hendricks, J., Jöckel, P., and Lohmann, U.: Global model simulations of the impact of ocean-going ships on aerosols, clouds, and the radiation budget, Atmos. Chem. Phys., 7, 5061–5079, doi:10.5194/acp-7-5061-2007, URL https://www.atmos-chem-phys.net/7/5061/2007/acp-7-5061-2007.html, 2007.

Liss, P. S. and Slater, P. G.: Flux of gases across the air−sea interface, Nature, 247, 181–184, URL http://dx.doi.org/10.1038/247181a0, 1974.

Liu, J., Xu, Y., Li, J., Liu, D., Tian, C., Chaemfa, C., and Zhang, G.: The distribution and origin of PAHs over the Asian marginal seas, the Indian, and the Pacific Oceans: Implications for outflows from Asia and Africa, J. Geophys. Res. (Atmos.), 119, 1949–1961, doi:10.1002/2013JD020361, URL http://onlinelibrary.wiley.com/doi/10.1002/2013JD020361/full, 2014.

Lohmann, R. and Lammel, G.: Adsorptive and absorptive contributions to the gas−particle partitioning of polycyclic aromatic hydrocarbons: State of knowledge and recommended parametrization for modeling, Environ. Sci. Technol., 38, 3793–3803, doi:10.1021/es035337q, URL http://pubs.acs.org/doi/pdfplus/10.1021/es035337q, 2004.

Lohmann, R., Klánová, J., Pribylova, P., Liskova, H., Yonis, S., and Bollinger, K.: PAHs on a west-to-east transect across the tropical Atlantic Ocean, Environ. Sci. Technol., 47, 2570–2578, doi:10.1021/es304764e, URL http://pubs.acs.org/doi/abs/10.1021/es304764e, 2013.

Ma, J., Daggupaty, S., Harner, T., and Li, Y.: Impacts of lindane usage in the Canadian prairies on the Great Lakes ecosystem. 1. Coupled atmospheric transport model and modeled concentrations in air and soil, Environ. Sci. Technol., 37, 3774–3781, doi:10.1021/es034160x, URL https://pubs.acs.org/doi/abs/10.1021/es034160x, 2003.

Mackay, D.: Multimedia environmental models: The fugacity approach, second edition, Taylor & Francis, URL http://books.google.de/books?id=f37zywrLJf0C, 2010.

Mackay, D. and Boethling, R. S.: Handbook of property estimation methods for chemicals: Environmental health sciences, Taylor & Francis, URL https://books.google.de/books?id=EhHutGUI3zwC, 2000.

MacLeod, M., Riley, W. J., and McKone, T. E.: Assessing the influence of climate variability on atmospheric concentrations of polychlorinated biphenyls using a global-scale mass balance model (BETR-global), Environ. Sci. Technol., 39, 6749–6756, doi:10.1021/es048426r, URL http://pubs.acs.org/doi/pdfplus/10.1021/es048426r, 2005.

MacLeod, M., von Waldow, H., Tay, P., Armitage, J. M., Wöhrnschimmel, H., Riley, W. J., McKone, T. E., and Hungerbuhler, K.: BETR global − A geographically-explicit global-scale multimedia contaminant fate model, Environ. Pollut., 159, 1442–1445, doi:10.1016/j.envpol.2011.01.038, URL http://www.sciencedirect.com/science/article/pii/S0269749111000601, 2011.

Malanichev, A., Mantseva, E., Shatalov, V., Strukov, B., and Vulykh, N.: Numerical evaluation of the PCBs transport over the Northern Hemisphere, Environ. Pollut., 128, 279–289, doi:10.1016/j.envpol.2003.08.040, URL http://www.sciencedirect.com/science/article/pii/S026974910300349X, 2004.

Matthias, V., Aulinger, A., and Quante, M.: CMAQ simulations of the benzo(a)pyrene distribution over Europe for 2000 and 2001, Atmos. Environ., 43, 4078–4086, doi:10.1016/j.atmosenv.2009.04.058, URL http://www.sciencedirect.com/science/article/pii/S1352231009003951, 2009.

Mu, Q., Shiraiwa, M., Octaviani, M., Ma, N., Ding, A., Su, H., Lammel, G., Pöschl, U., and Cheng, Y.: Temperature effect on phase state and reactivity controls atmospheric multiphase chemistry and transport of PAHs, Sci. Adv., 4, doi:10.1126/sciadv.aap7314, URL http://advances.sciencemag.org/content/4/3/eaap7314.abstract, 2018.

Nizzetto, L., Lohmann, R., Gioia, R., Jahnke, A., Temme, C., Dachs, J., Herckes, P., Guardo, A. D., and Jones, K. C.: PAHs in air and seawater along a North−South Atlantic transect: Trends, processes and possible sources, Environ. Sci. Technol., 42, 1580–1585, doi:10.1021/es0717414, URL http://pubs.acs.org/doi/abs/10.1021/es0717414, 2008.

O'Dowd, C. D., Langmann, B., Varghese, S., Scannell, C., Ceburnis, D., and Facchini, M. C.: A combined organic−inorganic sea-spray source function, Geophysical Research Letters, 35, L01 801, doi:10.1029/2007GL030331, URL https://agupubs.onlinelibrary.wiley.com/doi/full/10.1029/2007GL030331, 2008.

Pankow, J. F.: Review and comparative analysis of the theories on partitioning between the gas and aerosol particulate phases in the atmosphere, Atmos. Environ., 21, 2275–2283, doi:10.1016/0004-6981(87)90363-5, URL http://www.sciencedirect.com/science/article/pii/0004698187903635, 1987.

Perraudin, E., Budzinski, H., and Villenave, E.: Kinetic study of the reactions of ozone with polycyclic aromatic hydrocarbons adsorbed on atmospheric model particles, J. Atmos. Chem., 56, 57–82, doi:10.1007/s10874-006-9042-x, URL http://link.springer.com/article/10.1007/s10874-006-9042-x, 2007.

Pozzer, A., Jöckel, P., Sander, R., Williams, J., Ganzeveld, L., and Lelieveld, J.: Technical Note: The MESSy-submodel AIRSEA calculating the air−sea exchange of chemical species, Atmos. Chem. Phys., 6, 5435–5444, doi:10.5194/acp-6-5435-2006, URL http://www.atmos-chem-phys.net/6/5435/2006/, 2006.

Pringle, K. J., Tost, H., Message, S., Steil, B., Giannadaki, D., Nenes, A., Fountoukis, C., Stier, P., Vignati, E., and Lelieveld, J.: Description and evaluation of GMXe: a new aerosol submodel for global simulations (v1), Geosci. Model Dev., 3, 391–412, doi:10.5194/gmd-3-391-2010, URL http://www.geosci-model-dev.net/3/391/2010/, 2010.

Qureshi, A., MacLeod, M., and Hungerbühler, K.: Modeling aerosol suspension from soils and oceans as sources of micropollutants to air, Chemosphere, 77, 495–500, doi:10.1016/j.chemosphere.2009.07.051, URL http://www.sciencedirect.com/science/article/pii/S0045653509008789, 2009.

Roeckner, E., Bäuml, G., Bonaventura, L., Brokopf, R., Esch, M., Giorgetta, M., Hagemann, S., Kirchner, I., Kornblueh, L., Manzini, E., Rhodin, A., Schlese, U., Schulzweida, U., and Tompkins,

A.: The atmospheric general circulation model ECHAM 5. PART I: Model description, Report 349, Max-Planck-Institut für Meteorologie, Hamburg, URL http://edoc.mpg.de/175329, 2003.

Roeckner, E., Brokopf, R., Esch, M., Giorgetta, M., Hagemann, S., Kornblueh, L., Manzini, E., Schlese, U., and Schulzweida, U.: Sensitivity of simulated climate to horizontal and vertical resolution in the ECHAM5 atmosphere model, J. Climate, 19, 3771–3791, doi:10.1175/JCLI3824.1, URL https://journals.ametsoc.org/doi/pdf/10.1175/JCLI3824.1, 2006.

Sander, R., Baumgaertner, A., Gromov, S., Harder, H., Jöckel, P., Kerkweg, A., Kubistin, D., Regelin, E., Riede, H., Sandu, A., Taraborrelli, D., Tost, H., and Xie, Z. Q.: The atmospheric chemistry box model CAABA/MECCA-3.0, Geosci. Model Dev., 4, 373–380, doi:10.5194/gmd-4-373-2011, URL http://www.geosci-model-dev.net/4/373/2011/, 2011.

Scheringer, M. and Wania, F.: Multimedia models of global transport and fate of persistent organic pollutants, pp. 237–269, Springer Berlin Heidelberg, Berlin, Heidelberg, doi:10.1007/10751132_9, URL https://link.springer.com/content/pdf/10.1007%2F10751132_9.pdf, 2003.

Schulz, M., Balkanski, Y. J., Guelle, W., and Dulac, F.: Role of aerosol size distribution and source location in a three-dimensional simulation of a Saharan dust episode tested against satellite-derived optical thickness, J. Geophys. Res. (Atmos.), 103, 10 579–10 592, doi:10.1029/97JD02779, URL http://onlinelibrary.wiley.com/doi/10.1029/97JD02779/abstract, 1998.

Schwarzenbach, R. P., Gschwend, P. M., and Imboden, D. M.: Transport by Random Motion, pp. 777–832, John Wiley & Sons, Hoboken, NJ, USA, doi:10.1002/0471649643.ch18, URL http://dx.doi.org/10.1002/0471649643.ch18, 2005.

Sehili, A. M. and Lammel, G.: Global fate and distribution of polycyclic aromatic hydrocarbons emitted from Europe and Russia, Atmos. Environ., 41, 8301–8315, doi:10.1016/j.atmosenv.2007.06.050, URL http://www.sciencedirect.com/science/article/pii/S1352231007005833, 2007.

Semeena, V. S. and Lammel, G.: The significance of the grasshopper effect on the atmospheric distribution of persistent organic substances, Geophys. Res. Lett., 32, L07 804, doi:10.1029/2004GL022229, URL http://onlinelibrary.wiley.com/doi/10.1029/2004GL022229/full, 2005.

Semeena, V. S., Feichter, J., and Lammel, G.: Impact of the regional climate and substance properties on the fate and atmospheric long-range transport of persistent organic pollutants — Examples of DDT and γ-HCH, Atmos. Chem. Phys., 6, 1231–1248, doi:10.5194/acp-6-1231-2006, URL http://www.atmos-chem-phys.net/6/1231/2006/, 2006.

Shahpoury, P., Lammel, G., Albinet, A., Sofuoğlu, A., Dumanoğlu, Y., Sofuoğlu, S. C., Wagner, Z., and Zdimal, V.: Evaluation of a conceptual model for gas−particle partitioning of polycyclic aromatic hydrocarbons using polyparameter linear free energy relationships, Environ. Sci. Technol., 50, 12 312–12 319, doi:10.1021/acs.est.6b02158, URL http://pubs.acs.org/doi/pdfplus/10.1021/acs.est.6b02158, 2016.

Shen, H., Huang, Y., Wang, R., Zhu, D., Li, W., Shen, G., Wang, B., Zhang, Y., Chen, Y., Lu, Y., Chen, H., Li, T., Sun, K., Li, B., Liu, W., Liu, J., and Tao, S.: Global atmospheric emissions of polycyclic aromatic hydrocarbons from 1960 to 2008 and future predictions, Environ. Sci. Technol., 47, 6415–6424, doi:10.1021/es400857z, URL http://pubs.acs.org/doi/pdfplus/10.1021/es400857z, 2013.

Shiraiwa, M., Garland, R. M., and Pöschl, U.: Kinetic double-layer model of aerosol surface chemistry and gas−particle interactions (K2-SURF): Degradation of polycyclic aromatic hydrocarbons exposed to O3, NO2, H2O, OH and NO3, Atmos. Chem. Phys., 9, 9571–9586, doi:10.5194/acp-9-9571-2009, URL https://www.atmos-chem-phys.net/9/9571/2009/, 2009.

Shrivastava, M., Lou, S., Zelenyuk, A., Easter, R. C., Corley, R. A., Thrall, B. D., Rasch, P. J., Fast, J. D., Massey Simonich, S. L., Shen, H., and Tao, S.: Global long-range transport and lung cancer risk from polycyclic aromatic hydrocarbons shielded by coatings of organic aerosol, Proc. Natl. Acad. Sci., 114, 1246–1251, doi:10.1073/pnas.1618475114, URL http://www.pnas.org/content/114/6/1246.abstract, 2017.

Smit, A. A. M. F. R., Berg, F. v. d., and Leistra, M.: Estimation method for the volatilization of pesticides from fallow soil, DLO Winand Staring Centre, Wageningen, Netherlands, 1997.

Smit, A. A. M. F. R., Leistra, M., and Berg, F. v. d.: Estimation method for the volatilization of pesticides from plants, DLO Winand Staring Centre, Wageningen, Netherlands, 1998.

Stein, U. and Alpert, P.: Factor separation in numerical simulations, J. Atmos. Sci., 50, 2107–2115, doi:10.1175/1520-0469(1993)050<2107:FSINS>2.0.CO;2, URL http://journals.ametsoc.org/doi/abs/10.1175/1520-0469(1993)050%3C2107%3AFSINS%3E2.0.CO%3B2, 1993.

Thackray, C. P., Friedman, C. L., Zhang, Y., and Selin, N. E.: Quantitative assessment of parametric uncertainty in Northern Hemisphere PAH concentrations, Environ. Sci. Technol., 49, 9185–9193, doi:10.1021/acs.est.5b01823, URL http://dx.doi.org/10.1021/acs.est.5b01823, 2015.

Thibault, G. and Elliott, N.: Accelerating the biological cleanup of hazardous materials spills, pp. 115–120, 1979.

Tørseth, K., Aas, W., Breivik, K., Fjæraa, A. M., Fiebig, M., Hjellbrekke, A. G., Lund Myhre, C., Solberg, S., and Yttri, K. E.: Introduction to the European Monitoring and Evaluation Programme (EMEP) and observed atmospheric composition change during 1972−2009, Atmos. Chem. Phys., 12, 5447–5481, doi:10.5194/acp-12-5447-2012, URL http://www.atmos-chem-phys.net/12/5447/2012/, 2012.

Tost, H.: Global modelling of cloud, convection and precipitation influences on trace gases and aerosols, Ph.D. thesis, University of Bonn, URL http://hss.ulb.uni-bonn.de/2006/0731/0731.htm, unpublished thesis, 2006.

Tost, H., Jöckel, P., Kerkweg, A., Sander, R., and Lelieveld, J.: Technical Note: A new comprehensive SCAVenging submodel for global atmospheric chemistry modelling, Atmos. Chem. Phys., 6, 565–574, doi:10.5194/acp-6-565-2006, URL http://www.atmos-chem-phys.net/6/565/2006/, 2006a.

Tost, H., Jöckel, P., and Lelieveld, J.: Influence of different convection parameterisations in a GCM, Atmos. Chem. Phys., 6, 5475–5493, doi:10.5194/acp-6-5475-2006, URL https://www.atmos-chem-phys.net/6/5475/2006/, 2006b.

Tost, H., Jöckel, P., and Lelieveld, J.: Lightning and convection parameterisations — Uncertainties in global modelling, Atmos. Chem. Phys., 7, 4553–4568, doi:10.5194/acp-7-4553-2007, URL https://www.atmos-chem-phys.net/7/4553/2007/, 2007.

Tost, H., Lawrence, M. G., Brühl, C., Jöckel, P., The, G. T., and The, S.-O. D. A. T.: Uncertainties in atmospheric chemistry modelling due to convection parameterisations and subsequent scavenging, Atmos. Chem. Phys., 10, 1931–1951, doi:10.5194/acp-10-1931-2010, URL http://www.atmos-chem-phys.net/10/1931/2010/, 2010.

Tsimpidi, A. P., Karydis, V. A., Pozzer, A., Pandis, S. N., and Lelieveld, J.: ORACLE (v1.0): Module to simulate the organic aerosol composition and evolution in the atmosphere, Geosci. Model Dev., 7, 3153–3172, doi:10.5194/gmd-7-3153-2014, URL https://www.geosci-model-dev.net/7/3153/2014/, 2014.

UNEP: The 16 New POPs: An introduction to the chemicals added to the Stockholm Convention as Persistent Organic Pollutants by the Conference of the Parties, http://chm.pops.int/TheConvention/ThePOPs/TheNewPOPs/tabid/2511/Default.aspx, accessed on 01/08/2018, 2017.

van Noort, P. C. M.: A thermodynamics-based estimation model for adsorption of organic compounds by carbonaceous materials in environmental sorbents, Environ. Toxicol. Chem., 22, 1179–1188, doi:10.1002/etc.5620220601, URL http://onlinelibrary.wiley.com/doi/10.1002/etc.5620220601/full, 2003.

van Vuuren, D. P., Edmonds, J., Kainuma, M., Riahi, K., Thomson, A., Hibbard, K., Hurtt, G. C., Kram, T., Krey, V., Lamarque, J.-F., Masui, T., Meinshausen, M., Nakicenovic, N., Smith, S. J., and Rose, S. K.: The representative concentration pathways: an overview, Clim. Change, 109, 5, doi:10.1007/s10584-011-0148-z, URL https://link.springer.com/article/10.1007/s10584-011-0148-z, 2011.

Wania, F.: Modelling the fate of non-polar organic chemicals in an ageing snow pack, Chemosphere, 35, 2345–2363, doi:10.1016/S0045-6535(97)00312-3, URL http://www.sciencedirect.com/science/article/pii/S0045653597003123, 1997.

Wania, F. and Mackay, D.: The evolution of mass balance models of persistent organic pollutant fate in the environment, Environ. Pollut., 100, 223–240, doi:10.1016/S0269-7491(99)00093-7, URL http://www.sciencedirect.com/science/article/pii/S0269749199000937, 1999.

WHO: Health risks of persistent organic pollutants from long-range transboundary air pollution, Report EUR/03/5042687, World Health Organization, URL http://apps.who.int/iris/handle/10665/107471, 2003.

Zelenyuk, A., Imre, D., Beránek, J., Abramson, E., Wilson, J., and Shrivastava, M.: Synergy between secondary organic aerosols and long-range transport of polycyclic aromatic hydrocarbons, Environ. Sci. Technol., 46, 12 459–12 466, doi:10.1021/es302743z, URL http://pubs.acs.org/doi/pdfplus/10.1021/es302743z, 2012.

Figures and Tables

Table 1. Summary of MESSy process submodels used in the study

Submodel	Purpose	Reference
AEROPT	Aerosol optical properties	Lauer et al. (2007)
AIRSEA	Air−sea exchange	Pozzer et al. (2006)
CLOUD	ECHAM5 cloud and precipitation scheme as MESSy submodel	Roeckner et al. (2006) and references therein
CONVECT	Convection parameterizations	Tost et al. (2006b, 2010)
CVTRANS	Convective tracer transport	Tost (2006)
DDEP	Dry deposition of gases and aerosols	Kerkweg et al. (2006a)
GMXe	Aerosol dynamics and thermodynamics	Pringle et al. (2010)
JVAL	Rate of photolysis	based on Landgraf and Crutzen (1998)
LNOX	NO_x production from lightning	Tost et al. (2007)
MECCA	Tropospheric and stratospheric chemistry	Sander et al. (2011)
OFFEMIS	Offline emissions	Kerkweg et al. (2006b)
ONEMIS	Online emissions	Kerkweg et al. (2006b)
RAD	ECHAM5 radiation scheme as MESSy submodel	Roeckner et al. (2006); Jöckel et al. (2006)
SCAV	Scavenging of gases and aerosols	Tost et al. (2006a)
SEDI	Aerosol sedimentation	Kerkweg et al. (2006a)

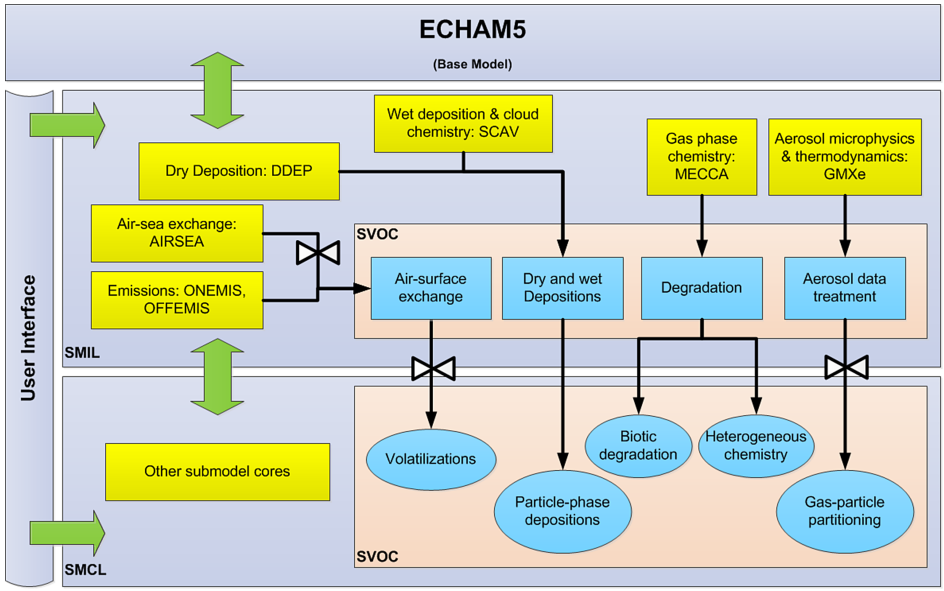

Figure 1. Overview of EMAC-SVOC model structure, the cycling processes in SVOC submodel and its interaction with other MESSy submodels. SMIL (submodel interface layer) and SMCL (submodel core layer) are components of MESSy coding standard, see (Jöckel et al., 2006) for further details.

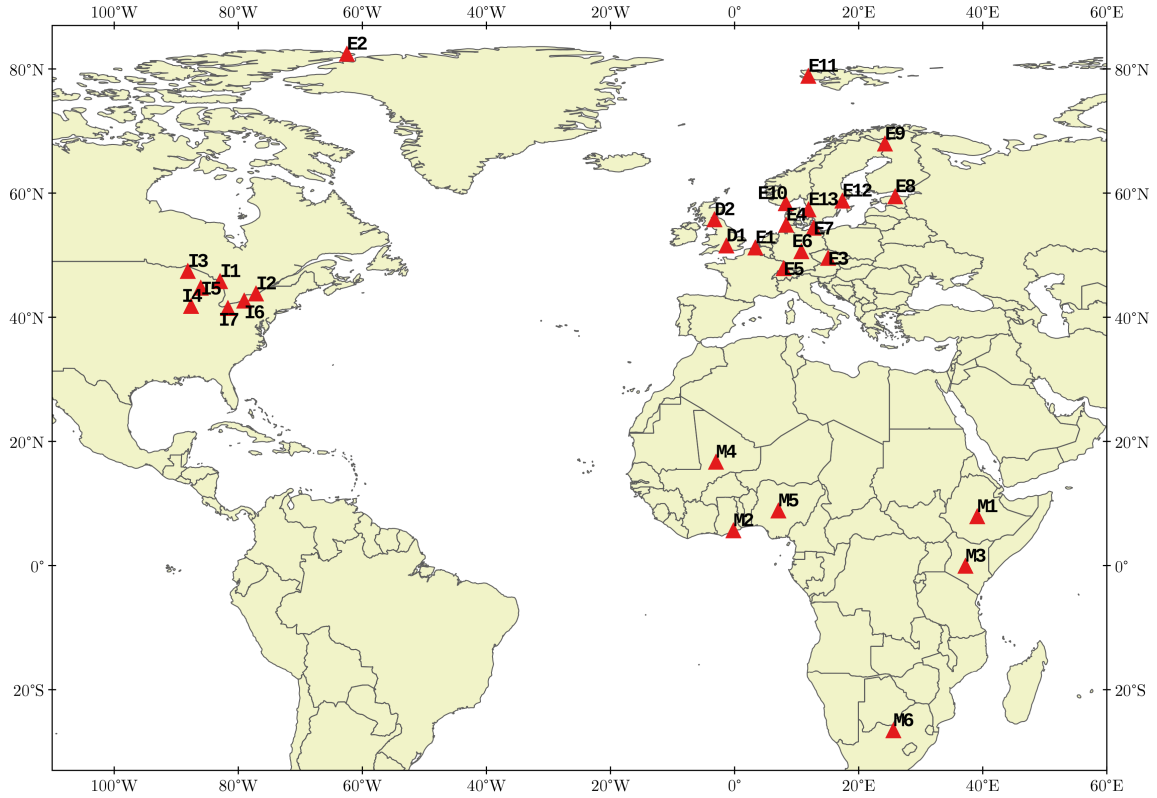

Figure 2. Locations of monitoring stations used in the study. The initial letter of each station ID refers to the individual monitoring network (E: EMEP & AMAP; D: DEFRA, I: IADN, M: MONET-Africa)

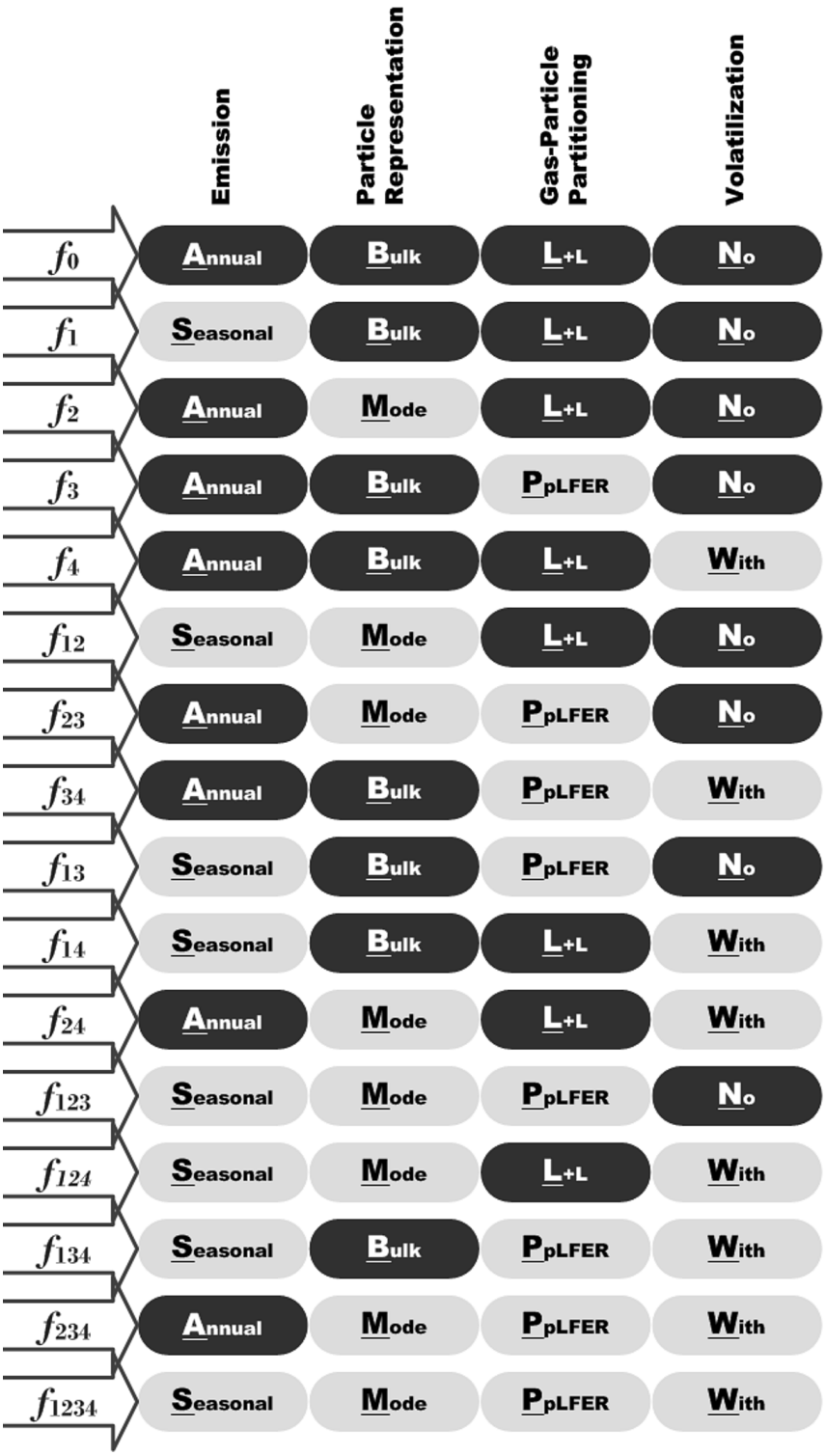

Figure 3. List of experiments performed for the factor separation analysis to study sensitivity to temporal variation in emission and process parameterizations (particulate-phase representation, gas−particle partitioning scheme, and volatilization). L+L: Lohmann−Lammel, ppLFER: Poly Parameter Linear Free Energy Relationships.

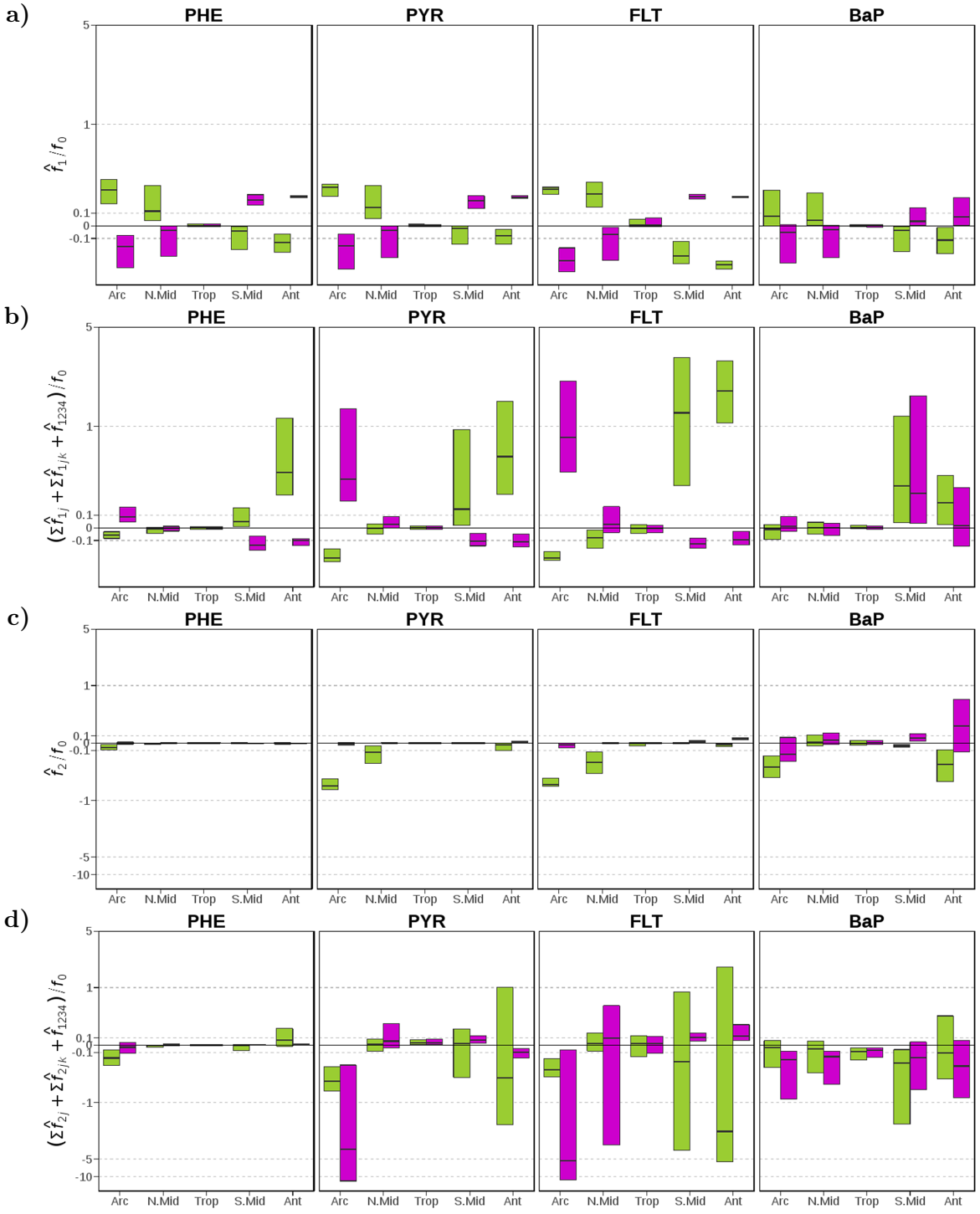

Figure 4. Direct and interaction effects on seasonal-mean near-surface PAH concentrations of (a,b) monthly emissions ($i = 1$), (c,d) the *modal* scheme ($i = 2$), (e,f) the ppLFER scheme ($i = 3$), and (g,h) volatilization ($i = 4$). The direct effects (a,c,e,g) are expressed as the difference between two distributions ($\hat{f}_i = f_i - f_0$) whereas the interaction effects (b,d,f,h) are expressed as the sum of two ($\Sigma\hat{f}_{ij}$, $i \neq j$), three ($\Sigma\hat{f}_{ijk}$, $i \neq j \neq k$), and all ($\hat{f}_{1234}$) factor interactions. They are presented as relative to concentrations from the *base* (f_0) simulation. The figures display the median, 25$^{\text{th}}$ and 75$^{\text{th}}$ percentiles of the relative effects over each of five main climatic regions. Note the inverse hyperbolic sine function has been used in scaling the y axes.

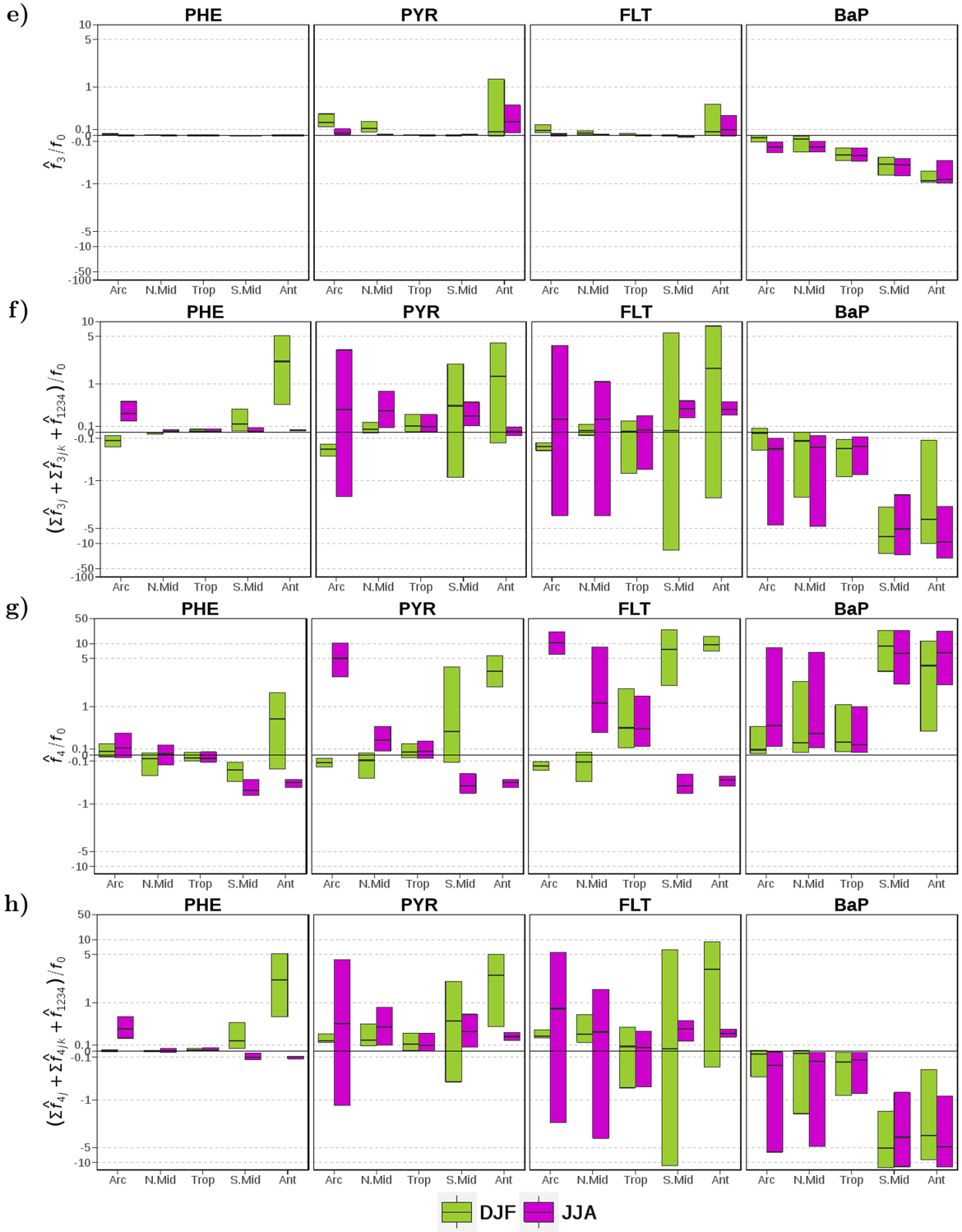

Figure 4. continued

Table 2. Statistics comparison of model simulation and observations of total (gas+particle) concentrations of PAHs from stations in the Arctic, northern mid-latitudes and tropics. N: Number of observed-simulated monthly data pairs; $\overline{x}$: Mean; $Q2_x$: Median; SD_x: Standard deviation; GM_x: Geometric mean; x: Simulated (M) or Observed (O) data; MB: Mean bias; RMSE: Root mean square error; NMB: Normalized mean bias; NMBF: Normalized mean bias factor; FAC2: Factor of 2; FAC10: Factor of 10; r: Correlation coefficient.

		Arctic				NH mid-latitudes				Tropics		
Metrics	**Unit**	**PHE**	**PYR**	**FLT**	**BaP**	**PHE**	**PYR**	**FLT**	**BaP**	**PHE**	**PYR**	**FLT**
N	months	89	89	89	46	361	328	372	405	34	34	34
$N_{<\mathrm{LOQ}}$	months	0	0	0	30	0	0	0	0	0	0	0
$\overline{O}$	ng m^{-3}	0.107	0.024	0.039	0.007	2.193	0.408	0.803	0.141	11.818	6.431	6.843
$Q2_O$	ng m^{-3}	0.034	0.014	0.012	0.002	1.301	0.194	0.360	0.037	3.608	2.106	2.181
SD_O	ng m^{-3}	0.162	0.027	0.054	0.015	2.956	0.582	1.135	0.253	16.598	10.141	10.217
GM_O	ng m^{-3}	0.051	0.014	0.018	0.003	0.968	0.221	0.383	0.046	3.733	1.369	1.726
$\overline{M}$	ng m^{-3}	0.046	0.025	0.079	5.2E−4	2.270	1.086	1.670	0.059	4.966	2.005	3.400
$Q2_M$	ng m^{-3}	0.010	0.007	0.034	1.9E−5	0.840	0.500	0.736	0.022	4.274	1.236	2.012
SD_M	ng m^{-3}	0.089	0.040	0.099	6.5E−4	2.955	1.225	2.007	0.085	3.897	2.019	3.462
GM_M	ng m^{-3}	0.012	0.008	0.041	3.4E−5	1.144	0.635	0.913	0.028	2.816	1.038	1.788
MB	ng m^{-3}	−0.060	0.001	0.040	−0.006	0.077	0.679	0.867	−0.083	−6.851	−4.426	−3.443
RMSE	ng m^{-3}	0.118	0.038	0.099	0.016	3.564	1.404	2.383	0.279	16.005	10.631	10.392
NMB	-	−0.56	0.06	1.04	−0.92	0.04	1.66	1.08	−0.58	−0.58	−0.69	−0.50
NMBF	-	−1.30	0.06	1.04	−12.17	0.04	1.66	1.08	−1.40	−1.38	−2.21	−1.01
FAC2	-	0.20	0.28	0.30	0.17	0.40	0.39	0.30	0.31	0.26	0.24	0.29
FAC10	-	0.82	0.90	0.94	0.33	0.90	0.84	0.83	0.79	0.97	0.79	0.85
r	-	0.83	0.42	0.42	0.16	0.27	0.23	0.09	0.01	0.63	0.33	0.29

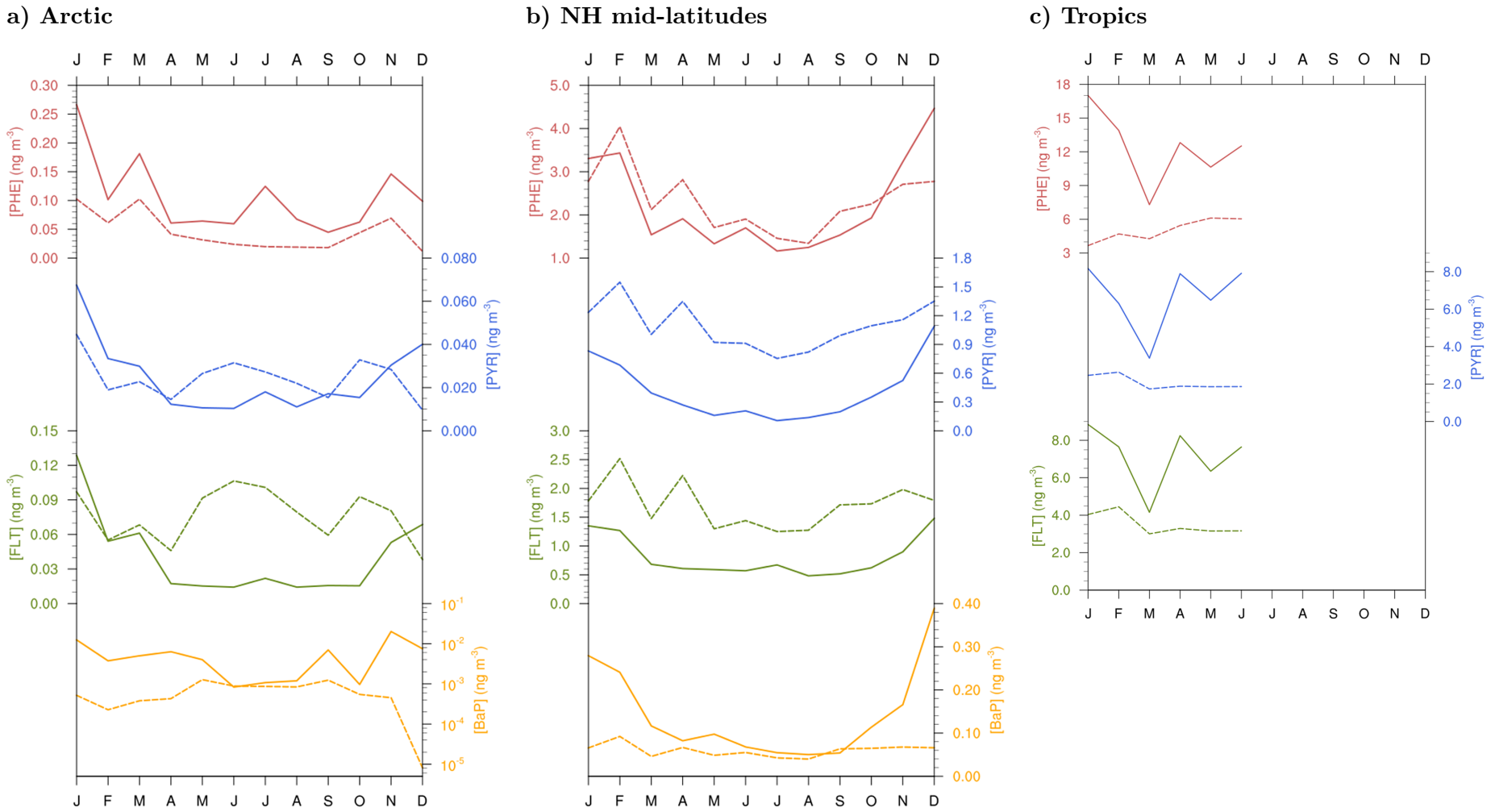

Figure 5. Seasonal mean total (gas+particle) concentrations of PAHs (ng m^{-3}) from observations (solid lines) and simulations (dashed lines) averaged over all stations in the (a) Arctic, (b) northern mid-latitudes, and (c) tropics. Note that logarithmic scale has been used for BaP concentrations in the Arctic.

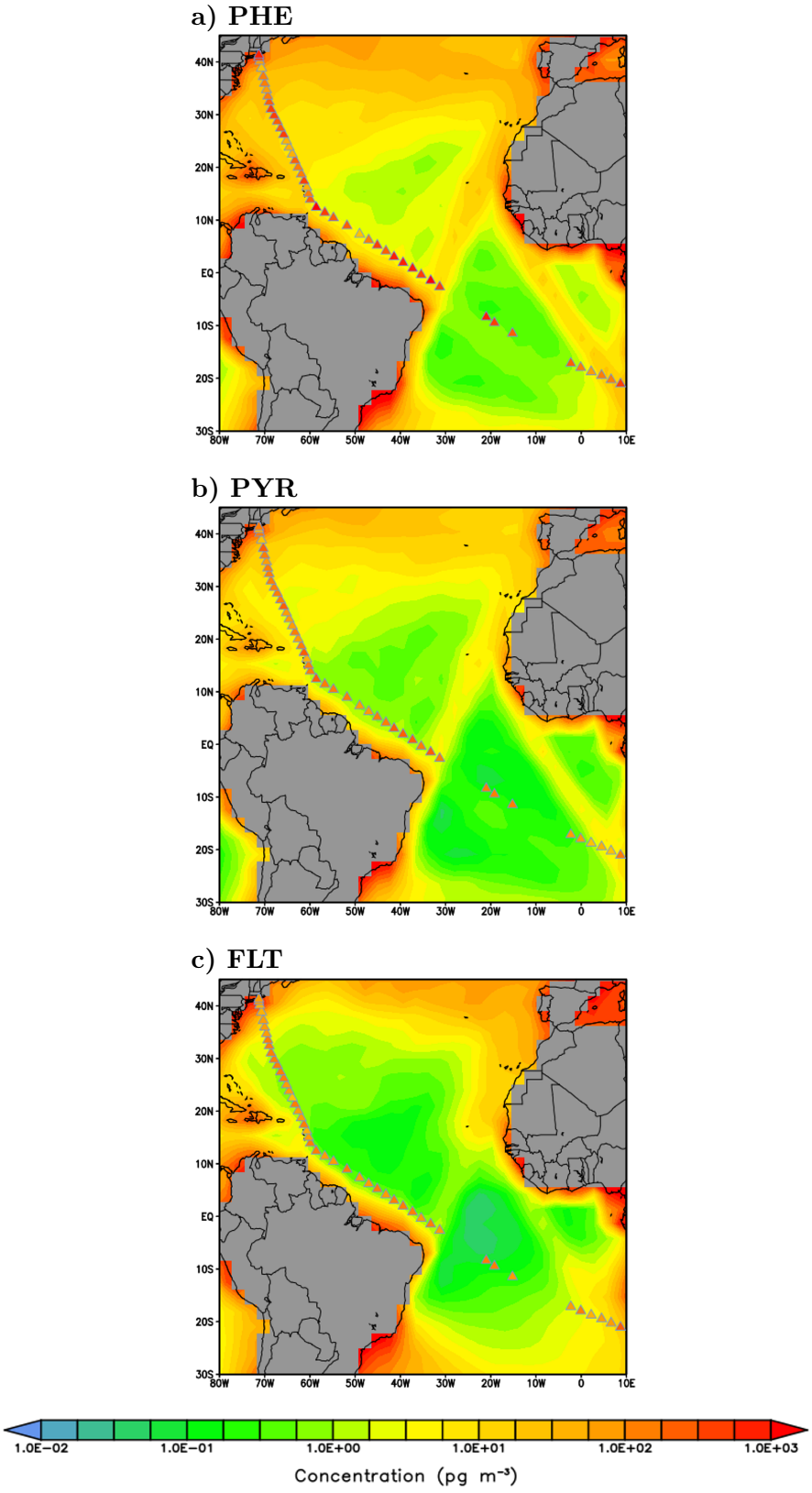

Figure 6. Simulated concentrations of PHE, PYR, and FLT (pg m^{-3}) over the Atlantic ocean overlaid with concentrations from a ship cruise measurement campaign during July 2009 (triangles). Land grid cells are depicted in gray shades.

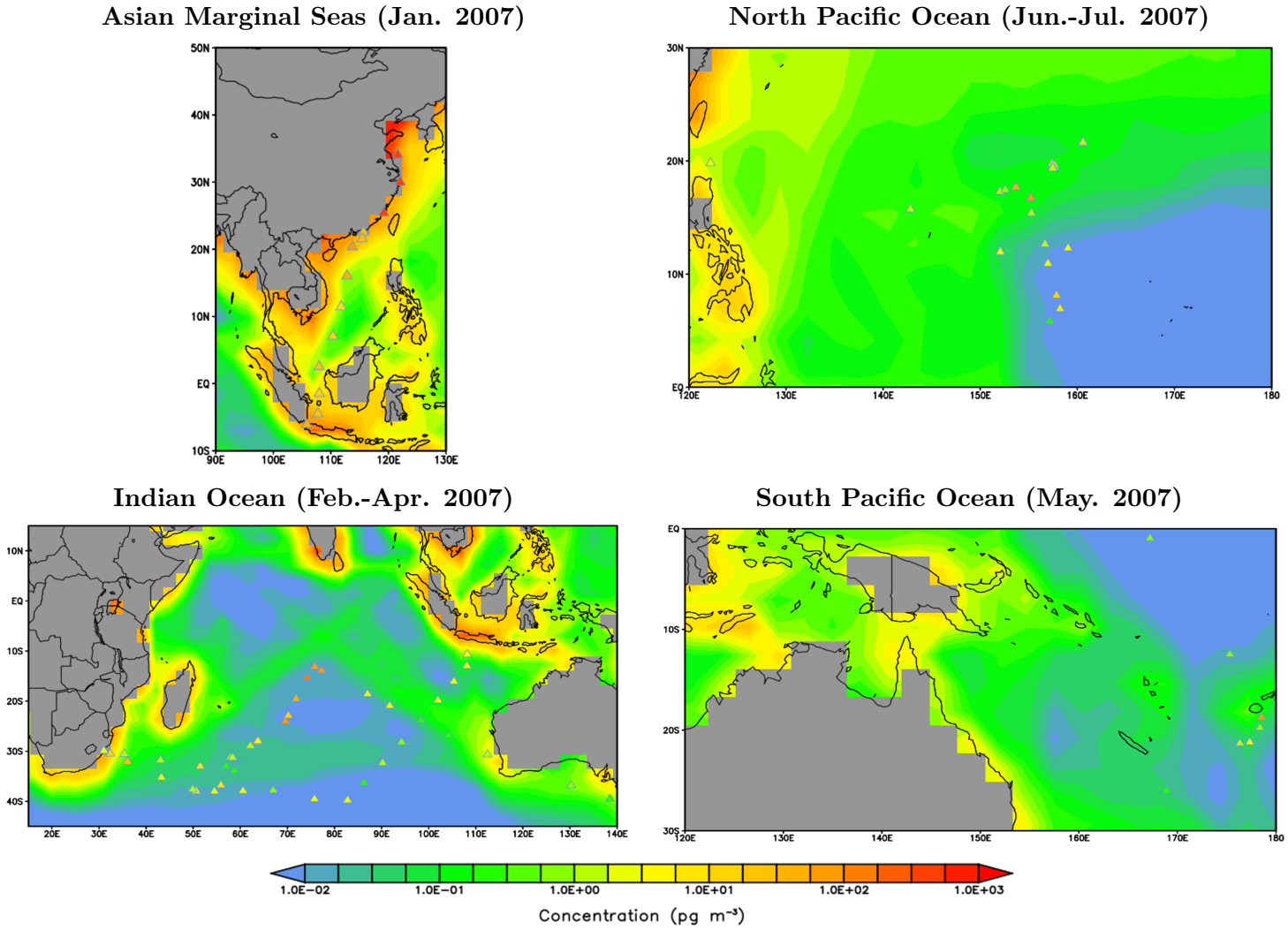

Figure 7. Simulated BaP concentrations (pg m^{-3}) over the four ocean margins overlaid with concentrations from a ship cruise measurement campaign (triangles). Land grid cells are depicted in gray shades.

Table 3. Statistics comparison of model simulation and observations of particulate mass fraction (θ) from a subset of surface stations, as listed in Table S11. N: Number of observed-simulated monthly data pairs; $\overline{x}$: Mean; SD_x: Standard deviation; x: Simulated (M) or Observed (O) data; MB: Mean bias; RMSE: Root mean square error; NMB: Normalized mean bias; NMBF: Normalized mean bias factor; FAC2: Factor of 2; FAC10: Factor of 10; r: Correlation coefficient.

Metrics	PHE	PYR	FLT	BaP
N	63	63	99	93
$\overline{O}$	0.051	0.359	0.268	0.949
SD_O	0.035	0.150	0.162	0.067
$\overline{M}$	0.005	0.212	0.106	0.964
SD_M	0.005	0.138	0.086	0.027
MB	−0.046	−0.147	−0.162	0.015
RMSE	0.057	0.214	0.225	0.074
NMB	−0.910	−0.410	−0.604	0.016
NMBF	−10.145	−0.694	−1.523	0.016
FAC2	0.00	0.56	0.30	1.00
FAC10	0.38	1.00	0.94	1.00
r	0.42	0.42	0.33	0.03

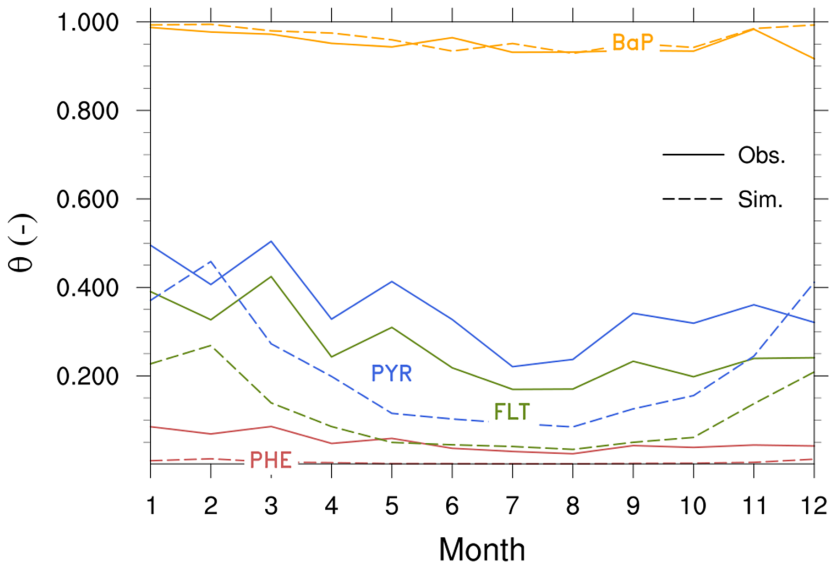

Figure 8. Seasonal mean particulate mass fraction (θ; unitless) from observations (solid lines) and simulations (dashed lines)